NORTHWESTERN UNIVERSITY

PASSIVE IMPLEMENTATION OF MULTIBODY SIMULATIONS FOR HAPTIC DISPLAY

A DISSERTATION

SUBMITTED TO THE GRADUATE SCHOOL
IN PARTIAL FULFILLMENT OF THE REQUIREMENTS

for the Degree

DOCTOR OF PHILOSOPHY

Field of Mechanical Engineering

by

J. Michael Brown

EVANSTON, ILLINOIS

December 1998

ABSTRACT

PASSIVE IMPLEMENTATION OF MULTIBODY SIMULATIONS
FOR HAPTIC DISPLAY

J. Michael Brown

The development of complex virtual environment simulations is a challenging problem in haptic display. Due to the dynamic interactions between the human operator, mechanism, sensors, actuators and physics-based simulation, provision of stability guarantees is both an interesting theoretical question and an important practical concern. Most existing virtual environments rely on the careful tuning of environment and control parameters to ensure stability. Whenever changes are made to the environment (such as changing the length of an object), these parameters have to be re-tuned. While merely annoying for relatively simple environments, this process becomes impractical for complex ones.

The focus of this work is the development of a software architecture that permits the simulation of complex multibody environments on a haptic display. This architecture separates the haptic display from the simulation, such that stability of the haptic display is not strongly dependent on simulation parameters. These simulations exhibit vastly improved stability properties compared to previous implementations. Since the haptic display and virtual environment are still weakly connected, guidelines for the design of virtual environments are presented.

Specifically, this thesis presents four distinct results associated with the proposed software architecture. The first result is a detailed passivity analysis of a 1 degree of freedom haptic display, generalizing previous analyses and providing design guidelines for the proposed software architecture. This result also substantiates discrete-time passivity as an exemplar for physics-based simulation methods. The second result is the establishment of a connection between the incremental conservation properties of physics-based numerical methods and discrete-time passivity of their numerical operators. This connection has important implications about which numerical methods are appropriate for use with haptic displays. The third result shows that discrete-time passive numerical operators require the solution of implicit equations. For reasons that are discussed, implicit equations are usually not solvable in real-time, making them difficult to use with haptic displays. The final result is an improved tuning procedure that preserves device passivity even with numerical methods that are not discrete-time passive.

ACKNOWLEDGMENTS

Top billing goes to my advisor, Ed Colgate, for providing me with an environment where I was allowed the freedom to roam. Because of this freedom, I have been forced to take more responsibility for myself and for the others around me. I've learned a lot about haptic displays and control, but I've learned a lot more about all sorts of other things, from teaching to writing to balancing family life with work.

Several other people deserve specific mention for their contributions to the work. Beeling Chang, whom I've had the pleasure to work alongside for almost six years, showed that the theory contained in this document is worthwhile by actually putting it into practice. Brian Miller, despite his recent arrival in the lab, caught up quickly, and has been invaluable in figuring out some of the more difficult concepts. He also played the important role of proofreader for much of this document. Brent Gillespie also took on this role, as well as providing all sorts of useful advice. Paul Millman left his fingerprints on much of the hardware in our lab, and because of that, it all still works. I would like to thanks the members of my doctoral committee -- Michael Peshkin, Scott Delp, and Randy Freeman -- for making sure that this document is technically sound and relevant. Finally, I would like to acknowledge Northwestern University's Cabell and Nugent Fellowship Programs, as well as the NASA Graduate Student Researchers Program, for providing financial support in the past six years.

On a personal level, I want to thank all the members of the Laboratory for Intelligent Mechanical Systems (and Social Policy?) for keeping things interesting, especially in the dog days of writing this document. Special thanks go to Carl Moore, who is constantly forcing me change the way I think about the world and my place within

it. Exalted Webmaster Bernie Reger has been a good friend and confidant ever since a fluids class many years ago. I'm also indebted to Witaya Wannasuphoprasit, Mike βrokowski, Don Cantrell, Andy Lorenz, Jon Lea, Julio Santos-Munné, Aaron Mills and Sang An for their friendship and counsel at various points in past several years.

Finally I'd like to thank my parents and sister for supporting my efforts for as long as I can remember, as well as Mick and Joan Howard for all their encouragement. Most of all, I want to thank Jodi for seven years of the best friendship I could ever hope for, and for teaching me that a life lived in fear is a life half-lived.

CONTENTS

CHAPTER 1
INTRODUCTION

This thesis involves the development of stable virtual environment simulations for haptic interfaces. A haptic interface comprises an input/output device (such as a force-feedback joystick or exoskeleton), a real-time controller, and a real-time simulation of a virtual environment. The controller collects information from the input/output device's sensors (position, velocity, force, and torque are the most common), which are then used as inputs to the simulation. The simulation estimates the forces the user should feel based on these sensor values and the internal state of the simulation itself. The simulation outputs are used by the controller to drive the input/output device's actuators. This type of system allows users to touch, feel, and manipulate virtual environments.

1.1 Background

Virtual reality in general, and haptic interface in particular, are driven by the desire for human interaction with various types of simulations. Depending on the purpose of the interaction, most applications fall within one of four major categories: training, manipulation, communication, and entertainment. Training applications include aeronautical (Colgate, et al. 1995) and surgical training (Basdogan, et al. 1998, Baumann, et al. 1996, Cotin, et al. 1996, Gibson, et al. 1996), rehabilitation (Hogan, et al. 1992), and education (Brooks, et al. 1990). The fundamental goal of the interaction is to allow the user to practice and learn in a safe, structured environment, perhaps providing haptic guidance along the way. Manipulation applications are centered around enhancing a user's ability to understand and control digitally stored information. Applications range from virtual prototyping (Nahvi, et al. 1998) and design (Stewart, et al. 1997) to novel user interfaces for commercial operating systems (e.g., Immersion Corporation's FEELIt™ mouse). In communication, two users are brought to a shared virtual environment (Buttolo, et al. 1996), or a single user manipulates a remote scene with the help of virtual fixtures (Rosenberg 1993). Entertainment applications take aspects of all three categories above, but the final goal is to provide enjoyment to the user, rather than to accomplish some commercially or socially motivated task. A separate non-commercial use of haptic displays is fundamental research into pyschophysics and human motion control (Durlach and Mavor 1994), which produces results that are important for all of the above applications.

Vision-based interaction, while quite useful for many applications, is sometimes insufficient to give the user a sense of immersion in the virtual environment. Certain simulations require sound to be effective, while others require haptic sensations. For example, if a medical student is learning how to perform a lumbar puncture, how the needle insertion feels is an important part of the task (Bostrom, et al. 1993). In training tasks in general, if the task to be learned requires manual dexterity or relies on haptic cues, then a haptic interface may enhance the training. In manipulation and communication tasks, the addition of haptic components can form a more natural interface to the virtual and remote environments. For example, in three dimensional CAD systems, it has been theorized that allowing a designer to interact haptically with an environment will enhance his or her ability to manipulate that environment (Hollerbach, et al. 1997). In entertainment applications, anecdotal evidence suggests that haptic interfaces are "cool", so that adding haptic sensations may improve their marketability.

1.2 State of the art

Many of the proposed applications for haptic interfaces involve the simulation of a complex dynamic system. This simulation must then be connected to a haptic display so that information about forces and motions can be exchanged haptically between the human user and the virtual environment. At the beginning of this project, however, virtual environments from published works had consisted primarily of haptic primitives, like virtual walls (Colgate, et al. 1993, Salcudean and Vlaar 1994) and simple textures (Howe and Cutkosky 1993, Klatzky, et al. 1989, Minsky 1995). Other implementations include (Zilles and Salisbury 1995), which describes an approach to point interaction with complex static environments, but does not address the extension to dynamic environments. Gillespie (Gillespie 1996) describes the implementation of complex dynamic environments whose constraint configurations are known a priori.

Notably missing from the haptics literature are general approaches to the interface between a haptic display and a complex dynamic simulation. This gap can be at least partially explained by the difficulty of providing *stability guarantees* when working with haptic virtual environments. These guarantees are important both because instabilities are potentially dangerous and because they typically destroy the user's sense of immersion. Most existing virtual environments rely on the careful tuning of environment and control parameters to ensure stability. Whenever changes are made to the environment (such as changing the length of an object), these parameters have to be re-tuned. While merely annoying for relatively simple environments, this process becomes impractical for complex ones. Additionally, current simulations are designed for a particular haptic display, and significant work is required to port the simulation over to a new device. As simulations become more complicated, perhaps being developed for multiple hardware configurations, this lack of portability becomes more important. Recent work by Adams et. al. (Adams and Hannaford 1998, Adams, et al. 1998) also addresses these issues, and in much the same spirit as the present work.

1.3 Goals of the work

As an avenue for exploring this topic, our group has begun developing hand tool simulations for use in aeronautical training systems. To help motivate this application, consider the recent use of virtual reality (VR) methods to train Space Shuttle support personnel in procedures involving highly specialized hand tools. While some tools used in micro-gravity are quite ordinary, others have unusual shapes and functions (e.g., various tools for emergency repairs). In the current VR training environment, tools are not represented at all, since this inclusion would require simulation of the interactions between virtual objects. For example, one merely points to a bolt that needs to be loosened, and it loosens itself. Clearly, this type of environment is useful for learning a complicated *procedure*, but not a physical *skill*. To develop a physical skill, haptic interaction is a necessary component of the training.

In light of the hand-tool-based environments we envision building, a general multibody simulation incorporates the required range of physical behaviors. Further, a simulation of this type would also be useful in virtual prototyping, and may form the basis for additional applications. Multibody simulations typically address at least a subset of the following characteristics:

- An environment comprising rigid polyhedra, springs, and dampers
- Bilateral (i.e. permanent) constraints, such as revolute and prismatic joints
- Unilateral constraints, such as collisions, sliding contact or rolling contact

In the effort to build complex multibody environments for haptic interface, a natural starting point is the physics-based simulation literature, where there have been countless publications covering the topics of numerical integration, collision detection, and collision response. This literature pulls from several different research communities: computer graphics, robotics, and applied mechanics. In recent years, it has produced a variety of modeling and implementation tools for use with multibody computer simulations. However, since these tools were not designed with haptic interface in mind, it is not clear that they will work properly when used in this context. For a review of multibody simulation formalisms and their applicability to haptic interface, see (Gillespie 1997).

Our own experience has indicated that algorithms which work well with stand-alone simulations often fail when implemented with a haptic display. The cause of this failure is the difficulty of obtaining stability guarantees for any usefully broad class of environments. To address this difficulty, it would be useful to develop a general-purpose software and hardware architecture for real-time haptic interaction between users and complex dynamic simulations. Ideally, this architecture would decouple the haptic display from the multibody simulation, such that stability of the haptic display is not strongly dependent on simulation parameters. Our goal is to allow a knowledgeable user (but not an expert in haptic display) to design virtual environments while maintaining confidence that the resultant system will be stable.

1.4 Contributions

In general terms, the contribution of the present work is the development of a general-purpose software architecture for real-time haptic interaction between users and complex dynamic simulations. This architecture separates the haptic display from the simulation, such that stability of the haptic display is not strongly dependent on simulation parameters. The separation also allows the simulation software to be ported easily from one device to another. Since the haptic display and virtual environment are still weakly connected, guidelines for the design of virtual environments are presented.

Specifically, this thesis makes four significant contributions to the field of haptic interface. The first is a detailed passivity analysis of a haptic display, generalizing previous analyses and providing design guidelines for the proposed software architecture. It also substantiates discrete-time passivity as an exemplar for physics-based simulation methods. The second contribution of the work is the establishment of a connection between discrete-time passivity and the incremental conservation properties of physics-based numerical methods. This connection has important implications about which numerical methods are appropriate for use with haptic displays. The third contribution of the work somewhat weakens the first - it is shown that discrete-time passive numerical operators require the solution of implicit equations. For reasons that will be discussed, implicit equations are usually not solvable in real-time, making them difficult to use with haptic displays. The final contribution is that, given restrictions on environment parameters, device passivity can sometimes be preserved even when using numerical methods that are not discrete-time passive. An important benchmark simulation is that of a point mass, and these restrictions take the form of a minimum mass that can be simulated passively. This development suggests a tuning procedure that can be used to guarantee stability over a wide range of virtual environments.

1.5 Organization of the document

Chapter 2 contains a selective review of terminology and basic theory associated with the passivity of sampled-data systems, and Chapter 3 reviews previous passivity analyses of haptic interfaces. Chapter 4 contains a generalization of prior passivity work, and provides guidelines for software design. Chapter 5 establishes the connection between discrete-time passivity and the conservation properties of physics-based simulation methods. Chapter 6 shows that discrete-time passive operators require the solution of implicit equations, and discusses why these equations are difficult to use with haptic displays. Chapter 7 explores the use of numerical methods that are not discrete-time passive, including a derivation of the minimum mass that can be simulated using specific explicit formulations. Finally, Chapter 8 summarizes the results and significance of the work and discusses some avenues for future research.

CHAPTER 2

REVIEW OF SAMPLED-DATA SYSTEMS AND PASSIVITY

The first section of this chapter reviews the basic concepts and notation used to describe the dynamics of *sampled-data* systems (systems which contain both continuous and discrete portions). The second section reviews the basic concepts, definitions and theorems of passivity analysis.

2.1 Sampled-data systems

`

Usually, a sampled-data system has a continuous-time plant (such as a motor), and a discrete-time controller (e.g. a computer or DSP chip). Conversions from continuous to discrete time are handled by an A/D converter, or sampler, which transmits the value of the continuous signal only at discrete (usually periodic) times. Conversions from discrete back to continuous time are handled by a D/A converter, or "hold" operator, which holds the discrete numbers over time to produce a continuous signal. The most common hold operator is a zero order hold (ZOH), which continually outputs the most recent number passed to its input.

Figure 2.1 shows an example of a sampled-data system with a continuous-time plant and a discrete-time controller.

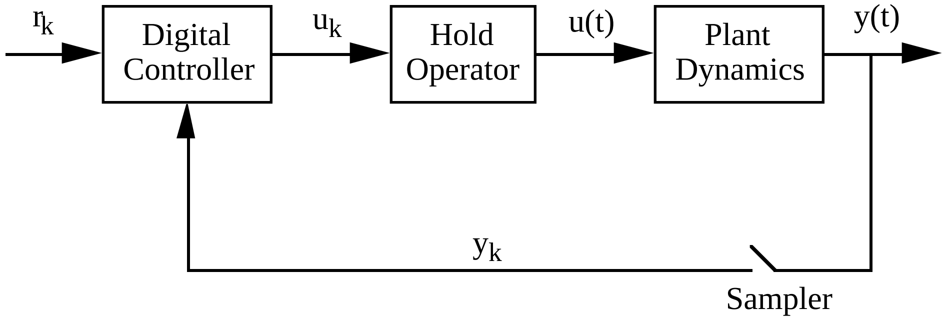

Figure 2.1. Diagram of a sampled data system. Continuous functions are represented with *f(t)*, whereas discrete functions are represented with f_k. The computed controller effort, u_k, becomes a continuous signal, *u(t)*, through the hold operator. The plant output, *y(t)*, is sampled, becoming y_k. In addition to the plant output, the digital controller acts on the discrete reference signal r_k.

The control effort *u(t)* and system output *y(t)* are continuous-time functions, and can be expressed as solutions of differential equations that represent the dynamics of the continuous system. The controller output u_k, the sampled output y_k, and the reference input r_k are discrete-time functions, and can be expressed as solutions of difference equations that represent the dynamics of the discrete system. It is important to understand that, in reality, discrete signals exist only as a train of numbers, and that difference equations operate on these signals without reference to time (i.e., time is a continuous concept, and is not well-defined in a purely discrete system).

In a sampled data system, however, these discrete signals interact with a continuous time system via the sample and hold process. In this domain, time does exist, and in fact is quite important in discussing the performance of the system. Thus, it is convenient to issue a "time stamp" that expresses when the discrete signals occur compared to continuous time events. Usually, periodic sampling is used, so we can express the time stamp as a multiple of the sampling time. Thus, y_k corresponds to the value of the output at the time *t=kT* and u_k is the controller output at the same instant of time.

Figure 2.2 demonstrates how linear continuous-time operators and signals may be represented with Laplace variables and functions, which encapsulate the frequency content of signals and linear operators via the Laplace Transform. Linear discrete-time operators and signals may be represented with pulse variables and functions, which use the Z-transform to encapsulate frequency content.

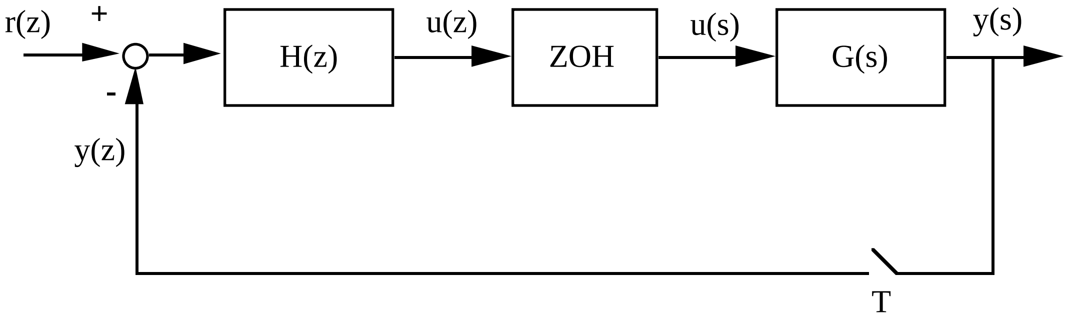

Figure 2.2. Block diagram of a linear sampled-data system with a zero order hold and periodic sampling. Continuous functions are represented in the Laplace domain with *f(s)*, and discrete functions are represented with *f(z)*.

A subtlety is that pulse variables are continuous time representations of discrete signals, so that while the actual discrete signal u_k is defined only at sample times, the pulse representation *u(z)* is a series of impulses, each with area u_k, separated by a continuous zero signal (see Figure 2.3). This representation is very convenient for sampled data systems because linear continuous time effects, like computational delay, can be mathematically represented in the discrete part of the system. These effects are not easily modeled using traditional difference equations.

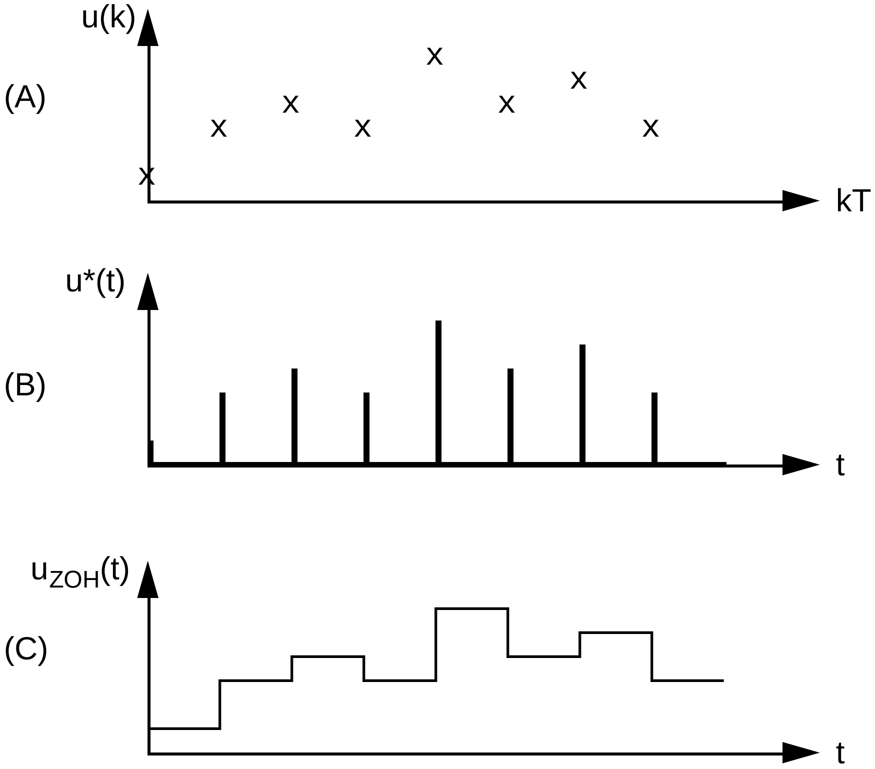

Figure 2.3. Representations of discrete signals. Original discrete signal (A), pulse variable description (B), signal after zero order hold (C).

Throughout this document, we will use linear models to describe the dynamics of the continuous-time portions of the system, so Laplace variables and functions will be sufficient. The discrete portions of our system, however, contain physics-based models of multibody systems. These models are often non-linear, so we will resort to difference equation descriptions of this portion of our system when necessary.

Figure 2.4 shows a block diagram representing the dynamics of a generic haptic display system. The human operator, actuators, mechanism, and sensors form the continuous-time portion of the system, while the virtual environment constitutes the discrete-time part of the system. The A/D and D/A form the interface between the continuous and digital domains of this sampled-data system.

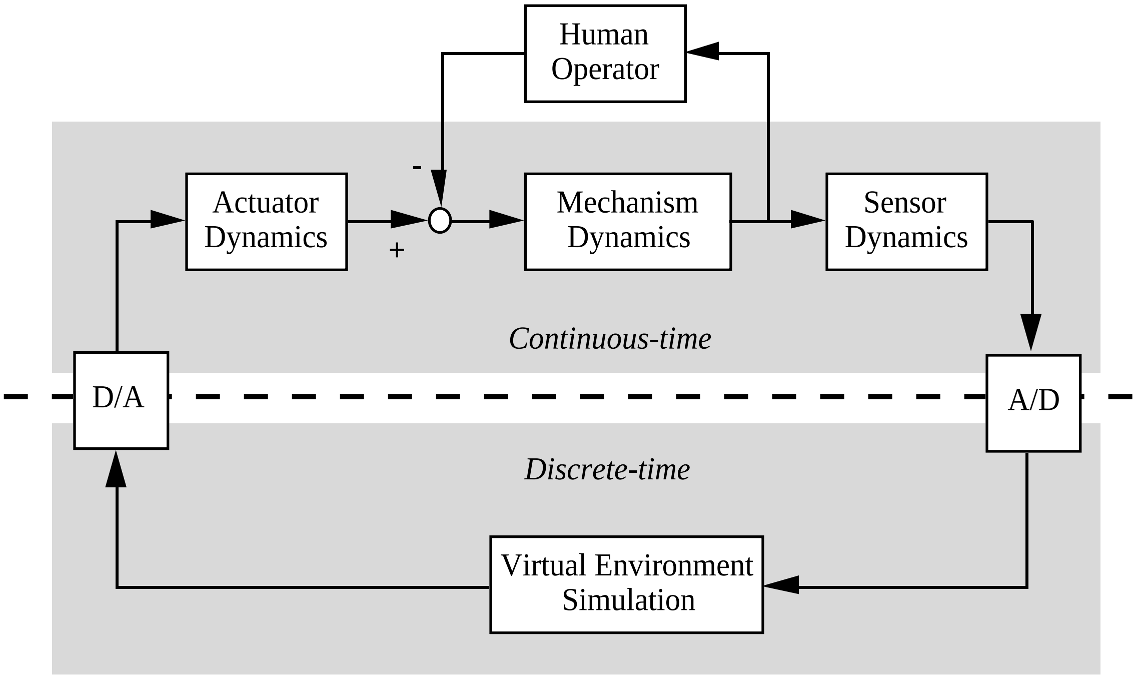

Figure 2.4. Generic block diagram a haptic display. The human, actuators, mechanism, and sensors are all continuous-time systems, while the virtual environment is a discrete-time system. The A/D and D/A form the interface between them. The shaded areas emphasize which parts of the haptic display are continuous vs. discrete time.

2.2 Basic passivity definitions, examples, and theory

This section reviews some basic concepts, definitions and theorems of passivity analysis. It is not intended to be a comprehensive introduction to passivity theory, but rather a very limited introduction to the specific results we will use throughout this document. A much more rigorous and comprehensive treatment can be found in (Desoer and Vidyasagar 1975, Khalil, et al. 1996). This section is divided into four parts: continuous-time systems, discrete-time systems, stability of coupled systems, and sampled-data systems.

2.2.1 Continuous-time systems

In this document, we only treat continuous-time systems that have linear dynamics, so that while there are powerful passivity tools for dealing with non-linear continuous-time systems, we will remain focused on the linear ones. Having said this, consider a generic (possibly non-linear) operator, *G*, which operates on an input signal, *u(t)*, resulting in the output signal *y(t)*. An intuitive definition of system passivity is that the maximum extractable energy be less than or equal to the initial stored energy. Translating this definition into more mathematical terms requires more information about the nature of the signals. However, we can make a mathematical statement about *operator* passivity without knowing anything about the nature of the signals. This statement by itself doesn't specify anything about energy, but can be a powerful analytical tool nonetheless. The operator *G* will be passive iff:

$$(2.1) \qquad \int_{t_0}^{t} u(t) \cdot y(t) dt \geq -E(t_0) \qquad \forall \text{ u(t)}, \forall \text{t} \geq \text{t}_0$$

where $E(t_0)$ is some constant that depends only on the initial conditions of the system. This mathematical statement of operator passivity matches the energy definition of system passivity when *u(t)* and *y(t)* are complimentary effort/flow variables. In this case, $u(t) \cdot y(t)$ is the instantaneous power delivered to the system, and *G* is defined as an impedance operator (i.e., it acts on effort to produce flow or, conversely, flow to produce effort).

If we further restrict *G* to be a linear operator, we can then describe it in the frequency domain via Parseval's Theorem. In this case, (2.1) simplifies to:

$$Re[\hat{G}(j\omega)] \geq 0 \qquad \forall\ \omega \in \Re \tag{2.2}$$

where $\hat{G}(j\omega)$ is the frequency-domain description of the operator *G*. Later in this section, we will use (2.2) to help generate passivity conditions on the continuous portion of the system.

2.2.2 Discrete-time systems

As in the previous section, consider a generic (possibly non-linear) operator, *G*, which operates on a discrete input signal, u_k, resulting in the discrete output signal y_k. Unlike the continuous-time case, we will not try to make an intuitive statement of system passivity for discrete systems. The problem is that the definition of extractable energy is arbitrary, even when u_k and y_k are an effort/flow pair. However, we can make a mathematical statement about *operator passivity* - the operator *G* will be passive iff:

$$\sum_{k=0}^{N} u_k \cdot y_k \geq -E_0 \qquad \forall\ u_k, \forall\ N \in \mathbb{Z}^+ \tag{2.3}$$

where E_0 is again a constant dependent on the initial conditions. Since much of our analysis deals with non-linear discrete-time simulations of dynamic systems, (2.3) will often be used for determining discrete-time passivity.

If we further restrict G to be a linear operator, we can describe it in the frequency domain via Parseval's Theorem:

$$\text{(2.4)} \qquad \mathrm{Re}[\tilde{g}(e^{j\theta})] \geq 0 \qquad \forall\theta \in [0, 2\pi]$$

where $\tilde{g}(e^{j\theta})$ is the discrete frequency-domain description of the operator G. It is important to remember that (2.4) will be of limited usefulness due to the restriction that G be a linear operator. However, it will be used as a shortcut to (2.3) in several examples later in this document. Having established the definitions for energetic passivity and operator passivity for both the continuous-time and the discrete-time cases, we turn to the Passivity Theorem and its corollaries in order to understand the interactions between passivity and coupled stability.

2.2.3 Stability of coupled systems

Consider the system shown in Figure 2.5, which shows the coupling of two (possibly non-linear) systems G and H. The Passivity Theorem states that if G is *input and output strictly passive,* but otherwise arbitrary, then a necessary and sufficient

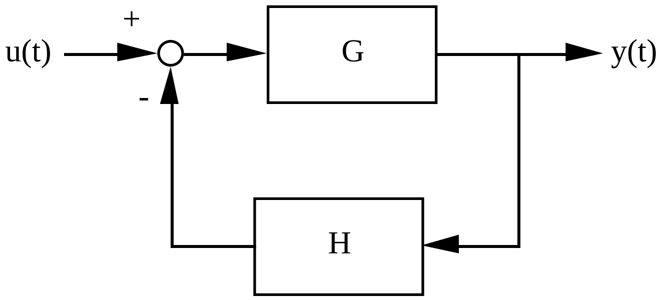

Figure 2.5. Block diagram showing the connection of two operators, where G is strictly passive (but otherwise arbitrary), and H is a system to which it is connected. Signals *u(t)* and *y(t)* do not have to be a complimentary effort/flow pair.

condition for coupled stability is the passivity of *H*.* This result seems intuitive, since neither system can continually generate energy needed for unstable oscillations. A corollary to the theorem is that if *G* is strictly passive (but otherwise arbitrary), then a necessary and sufficient condition for the passivity of *H* is that the coupled system be guaranteed stable. In practice, however, it is difficult to formulate stability guarantees for systems containing arbitrary non-linear operators. A direct derivation of passivity conditions using (2.1) or (2.3) is more appropriate for this type of proof.

If *G* is a linear passive (but otherwise arbitrary) impedance, then stability of the coupled system is easier to prove, and this is the approach taken below. It is important to note, however, that stability of the coupled system provides only a *necessary* condition for the passivity of *H*. Even though the system is stable, *H* might still be active, but the linear operator *G* will have no way of extracting the energy necessary to identify it as active. If *H* is linear, then the condition again becomes necessary and sufficient.

***Input and output strict passivity* is a slightly more demanding condition than that specified in (2.1) and (2.3). If the operator in question is linear, then (2.2) and (2.4) apply, but with the left hand side positive and uniformly bounded away from zero. Throughout this document, *stability* should be interpreted as finite gain input/output stability in the 2-norm, unless otherwise specified. Details of these conditions can be found in (Khalil, et al. 1996).

CHAPTER 3

REVIEW OF PREVIOUS PASSIVITY ANALYSES OF HAPTIC DISPLAYS

A primary goal of virtual environment simulations, whether haptic or visual, is to achieve a sense of "presence" in the virtual environment (Slater and Usoh 1993). If the state of that environment becomes computationally unstable, the sense of presence will be damaged, if not completely destroyed (imagine if a wrench began oscillating uncontrollably against a nut). Thus, virtual environment simulations, whether haptic or visual, need to provide stability guarantees. Our experience has shown that, for haptic display, stability guarantees are one of the most challenging aspect of virtual environment implementation.

The difficulty in any traditional stability analysis of this system is the unmodeled dynamics of the human operator. Even though the virtual environment itself might be stable, interaction with a human operator via a haptic interface may *cause* instability. In our studies of virtual environments, we have had many experiences with human operators adjusting their own behavior until oscillations resulted. Another approach to proving robustness is to derive the conditions under which the haptic display handle appears passive to the human operator. Under these conditions, the device cannot generate energy continually over time, making actuator-driven instabilities impossible. The following sections outline past theoretical approaches to achieving this goal.

3.1 Passivity of virtual environments with linear dynamics

For the past several years, our group has been using passivity as a tool to explore the performance of haptic displays. The foundation for this work was laid in (Colgate and Schenkel 1997), which developed necessary and sufficient conditions under which a haptic display with linear virtual environment dynamics will appear passive. The result was extended to include the effect of a unilateral constraint operator acting on the environment. Figure 3.1 shows the system model used in the analysis:

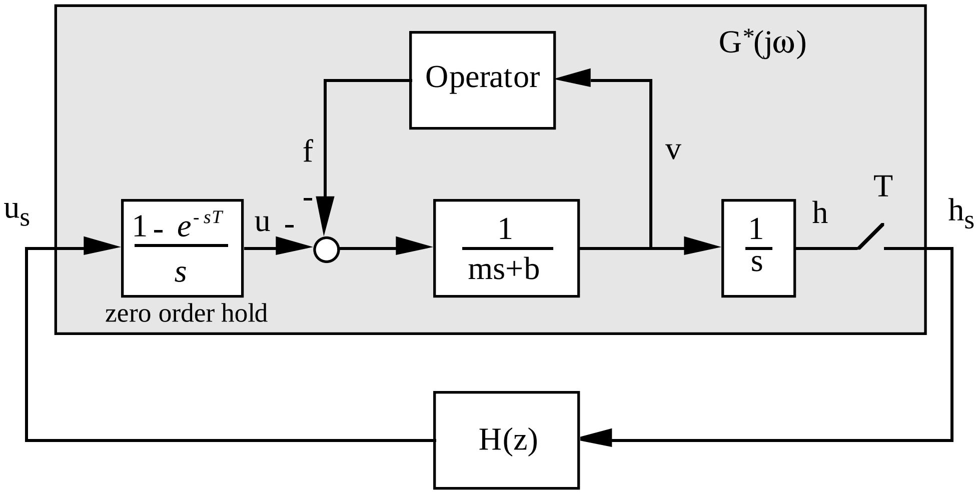

Figure 3.1. Colgate and Schenkel's model of a 1 DOF haptic display. Parameters *m* and *b* are the inherent inertia and damping of the haptic display handle. *H(z)* is the virtual environment, *T* is the sample time, *h* is the handle position and *u* is the actuator effort (h_S and u_S after sampling).

With the goal of understanding the effects of inherent manipulandum dynamics and sample-and-hold on the achievable dynamic range of haptic displays, Colgate and Schenkel developed a simple model that still captured the salient features of these components. This model has one degree of freedom and uses an ideal actuator, position sensor, sampler and zero order hold. The model of the mechanism dynamics approximates the behavior of the 1 DOF device in our laboratory.

The analytical approach was to replace the human operator with an arbitrary linear time-invariant passive (ALTIP) impedance and then derive the conditions under which the coupled system had to be stable. According to the Passivity Theorem (see §2.2.3), stability when connected to an ALTIP impedance provides a necessary and sufficient condition for the passivity of the haptic display. Insight into the derivation of these passivity conditions can be obtained graphically through a Nyquist-style analysis. Figure 3.2 shows a progression of transfer function and their corresponding regions in the Nyquist plane:

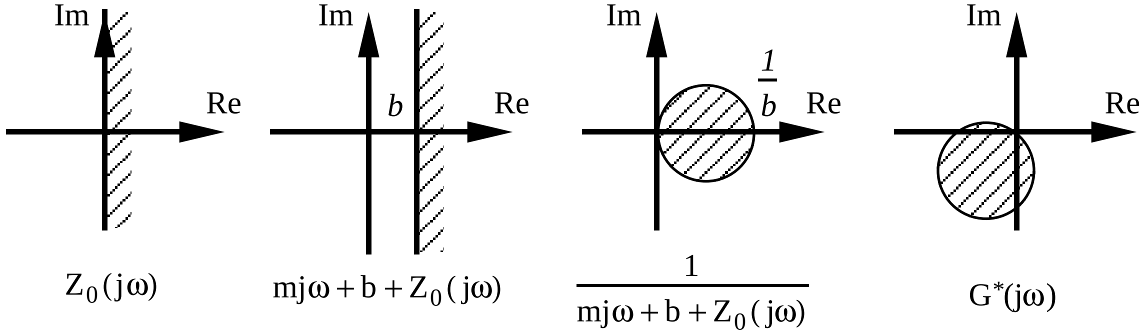
Im
Re
Im
b
Re
Im
1/b
Re
Im
Re
$Z_0(j\omega)$
$mj\omega + b + Z_0(j\omega)$
$\frac{1}{mj\omega + b + Z_0(j\omega)}$
$G^*(j\omega)$

Figure 3.2. Graphical representation of passivity derivation. Regions corresponding to the ALTIP impedance, mechanism, and sample/hold dynamics are shown in the Nyquist plane.

The ALTIP impedance, *$Z_0(j\omega)$*, occupies the entire right half-plane. Through a series of *Möbius transformations*[*] , the effects of additional dynamics are incorporated. Adding the mass and damping of the mechanism translates the half-plane to the right by the

[*] A Möbius transformation (also known as a bilinear transformation or a linear fractional transformation) is a specific type of conformal map, consisting of translations, rotations, magnifications, and inversions. It has the property that circles and lines always map to circles or lines. Disks, half-planes and holes always map to disks, half-planes or holes.

amount of damping *b*. Since the desired mapping is from force to velocity, this half-plane must be inverted, yielding a disk of radius $\frac{1}{2b}$, centered at $\frac{1}{2b}$ on the real axis.

The primary difficulty in this analysis is modeling the effects of sample and hold on the transfer function from u_S to h_S. Using the impulse model of sampled systems and the zero order hold model shown above, $G^*(s)$ is given by an infinite series:

$$G^*(s) = \frac{1}{T}\sum_{k=-\infty}^{+\infty} G(s + jn\omega_s) \qquad \omega_s = \frac{2\pi}{T} \tag{3.1}$$

$$G(s) = \frac{1 - e^{-Ts}}{s^2}\frac{1}{ms + b + Z_0(s)} \tag{3.2}$$

Because the disk of the previous step is frequency-independent, it can be removed from the summation in (3.1):

$$G^*(s) = \frac{1}{T}\frac{1}{ms + b + Z_0(s)} \cdot \sum_{k=-\infty}^{+\infty} \frac{1 - e^{-T(s + jn\omega_s)}}{(s + jn\omega_s)^2} \tag{3.3}$$

The remaining summation has a closed form, resulting in the following transfer function:

$$G^*(j\omega) = \frac{T}{2}\frac{e^{-j\omega T} - 1}{1 - \cos\omega T} \cdot \frac{1}{mj\omega + b + Z_0(j\omega)} \tag{3.4}$$

The last term in this expression is the unrotated disk shown in Figure 3.2. The terms in front are an additional Möbius Transformation, resulting in a scaled and rotated disk. At each frequency, the center and radius of the disk are:

$$\text{Center}\left\{G^*(j\omega)\right\} = \frac{T}{4b}\frac{e^{-j\omega T}-1}{1-\cos\omega T} \tag{3.5}$$

$$\text{Radius}\left\{G^*(j\omega)\right\} = \frac{T}{4b}\left|\frac{e^{-j\omega T}-1}{1-\cos\omega T}\right| \tag{3.6}$$

Having fully identified the region, a Möbius Transformation that maps this disk to the complete interior of the unit disk, pointwise in frequency, can be found. Finally, Colgate (Colgate 1994) found a related transformation that, when applied to H(z), results in a system with the same closed loop characteristic equation as the original. The Small Gain Theorem was then used to obtain necessary conditions for closed loop stability:

$$b > \frac{T}{2}\frac{1}{1-\cos\omega T}\text{Re}\left\{(1-z^{-1})H(z)\right\}_{z=e^{j\omega T}} \qquad 0 \le \omega \le \omega_N \tag{3.7}$$

where $\omega_N=\pi/T$ is the Nyquist frequency. An application of Parseval's Theorem was used to show that (3.7) is also a sufficient condition for closed loop stability of this system. Finally, it was proved that (3.7) remains unchanged if the virtual environment is preceded by a unilateral constraint operator.

This result can be used, for example, to investigate one implementation of a virtual wall:

$$H(z) = K + \frac{B}{T}\left(1-z^{-1}\right) \tag{3.8}$$

where *K* is the virtual stiffness and *B* is the virtual damping. When substituted into (3.7), the passivity condition simplifies to:

$$\text{(3.9)} \qquad b > \frac{KT}{2} + |B|$$

This result is important because it provides design guidelines for the mechanism dynamics of a haptic display. It shows that increasing the inherent physical damping of the mechanism will increase the maximum stiffness and damping the device can emulate. Further, it indicates that negative virtual damping can be used to cancel out the effect of the added physical damping when the stiffness is zero (i.e., the human operator has moved outside the wall).

An offshoot of this work was the use of a new performance measure for haptic displays: the "Z-width" (Colgate and Brown 1994). The Z-width of a haptic display is the range of impedances that it can simulate passively. This measure can be used to contrast different devices, even if they have different configurations. It can also be used along with a measure of simulation quality to compare different implementations of a given virtual environment. The Z-width is affected by a number of factors, including inherent mechanism dynamics, controller update rate, and sensor/actuator performance. To ensure system robustness, the haptic display hardware should never be commanded to render an impedance that is outside its Z-width.

While quite helpful for providing manipulandum design guidelines, (3.7) is not usually very effective for designing virtual environments. Along with the restriction to linear virtual environments, the result doesn't inherently apply to any well-defined class of virtual environments. Any proposed environment must be substituted into these conditions to see if its implementation will be passive. To move beyond these difficulties, we need to develop a framework for implementing a wider class of virtual environments.

3.2 Passivity of environments with a virtual coupling and linear dynamics

Extension of the virtual wall model to more complicated environments is often not a trivial task. When a haptic display has both translational and rotational degrees of freedom, even simple virtual environments generate instabilities if implemented unwisely. The problem is keeping the device within its Z-width. For example, consider a peg in hole simulation implemented on a 3-DOF planar haptic display (Figure 3.3).

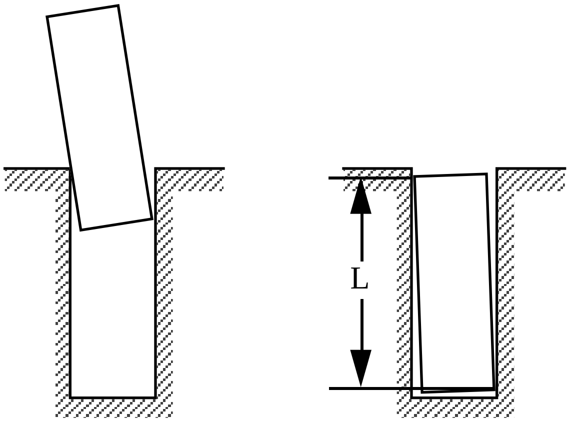

Figure 3.3. Two configurations of a peg in hole simulation. In this implementation, the massless, perfectly rigid peg tracks the handle of the haptic display. The hole is mechanically grounded and has a contact stiffness of K_C. The vertical distance between the contact points is L.

We can obtain the Z-width of the device either through derivation or experimental measurement. This Z-width is expressed as a three-element vector $[K_x\ K_y\ K_\theta]^T$, representing the maximum stiffness implementable across the entire workspace (neglecting for now the role of virtual damping). One approach to keeping the hardware within its Z-width is to model the peg as a massless rigid body that tracks the handle of the haptic display, while the hole is compliant. If the peg penetrates any surface, a reaction force/torque about the center of mass is computed according to the contact stiffness, K_c, and applied to the handle. In the second configuration of Figure 3.3, the stiffness matrix of the peg (and thus the handle of the haptic display) is given by:

$$\mathbf{K_{peg}} = \begin{bmatrix} K_c \\ 0 \\ \frac{1}{2} K_c L^2 \end{bmatrix} \tag{3.10}$$

There are two problems that make this approach infeasible. First, the rotational and translational components of the stiffness are interdependent (i.e., typically only one component can be set to its maximum stiffness for a given simulation). The other component will either be too compliant or exceed the Z-width of the device. Second, the stability of this simulation is geometry-dependent. For a given contact stiffness, it is always possible to choose a peg length that will result in severe instability. This second problem becomes even worse as simulations become more complicated, due to the increase in the number of parameters that strongly affect stability. A successful implementation needs to utilize the full Z-width of the device, while maintaining stability independent of simulation geometry. Finally, simulations in this framework must be designed for a particular device, resulting in poor simulation portability.

In (Colgate, et al. 1995), a more general approach to the implementation of complex virtual environments was developed. While the analysis was restricted to environments with linear dynamics, an important new concept was incorporated: *the virtual coupling*. Shown in Figure 3.4 as a spring and damper, the virtual coupling allows the environment design to be separated from the sampled-data control issues associated with haptic display. The virtual coupling is a multi-dimensional compliant element that is placed between the haptic display hardware and the virtual tool. Acting as an impedance filter, the virtual coupling limits the rendered impedances to within the Z-width of the particular device being used. If the virtual environment calls for an infinite stiffness to be displayed, such as when a rigid wrench interacts with a rigid bolt, the device will instead render the impedance of the virtual coupling.

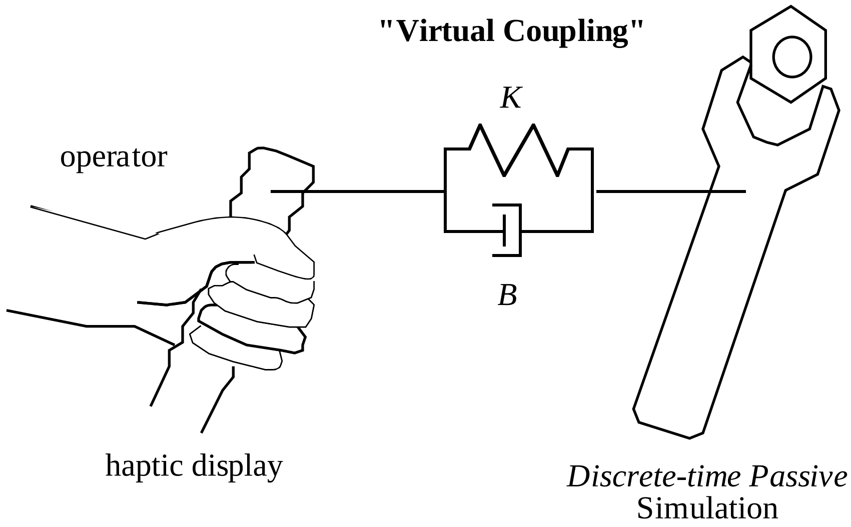

Figure 3.4. Conceptualization of a virtual coupling in a hand tool simulation.

The 1 DOF model shown in Figure 3.5 was used to demonstrate the effectiveness of this approach. In this model, the virtual coupling is a 2-port operator, where each element contains a backwards difference discretization of a spring-damper.

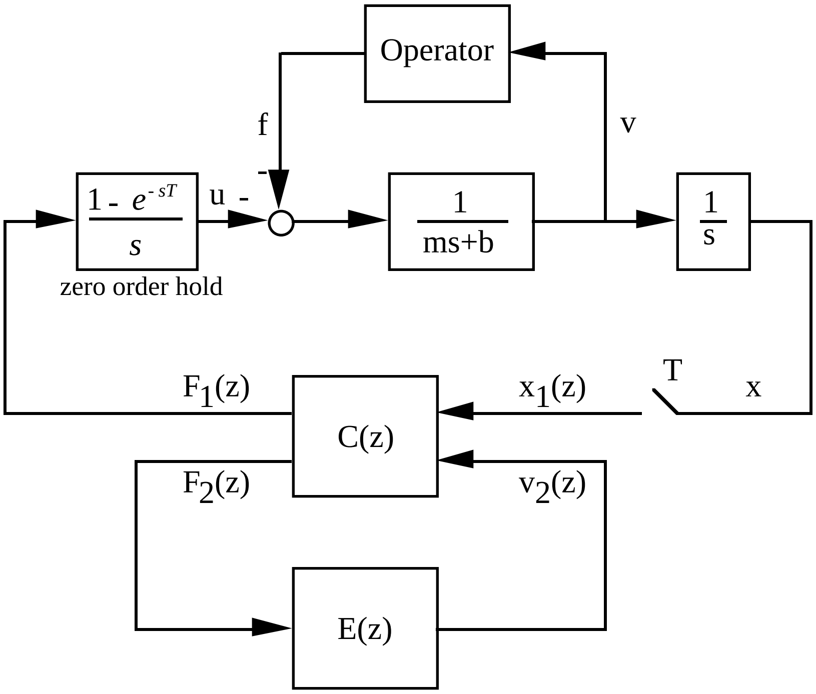

Figure 3.5. Block diagram of a 1 DOF haptic display using a virtual coupling. The virtual coupling and environment are represented by *C(z)* and *E(z)*, respectively. The human operator, as in previous work, is replaced with an arbitrary linear time-invariant passive operator.

The mappings go from endpoint position and virtual environment velocity to force, with the two forces being equal and opposite because they represent the force between the haptic display handle and virtual environment.

$$\begin{bmatrix} F_1(z) \\ F_2(z) \end{bmatrix} = \begin{bmatrix} K + \frac{B}{T}\left(1 - z^{-1}\right) & \frac{-KT}{1 - z^{-1}} - B \\ -K - \frac{B}{T}\left(1 - z^{-1}\right) & \frac{KT}{1 - z^{-1}} + B \end{bmatrix} \begin{bmatrix} x_1(z) \\ v_2(z) \end{bmatrix} \tag{3.11}$$

Using structured singular values, it was demonstrated that the conditions under which this system is stable are the same as for the virtual wall (3.9). This result is useful because it extends the virtual wall result to a significantly wider class of virtual environments -- those with linear discrete-time passive dynamics.

The scope of the result is limited, however, because the analysis applies only to the particular virtual coupling given in (3.9). It would be preferable to have a more general result like (3.5), which could then be used as a tool for designing both virtual couplings and environments. A second limitation is the analysis only addresses simulations with linear dynamics, whereas many of the systems we wish to simulate are highly non-linear. The final limitation is that the output of a numerical simulation is likely to contain position information, while the analysis above assumes velocity is the output. The next chapter presents a generalized version of the virtual coupling, and will address the issues mentioned above.

CHAPTER 4

PASSIVE IMPLEMENTATIONS OF HAPTIC VIRTUAL ENVIRONMENTS

The developments that follow will continue to use the virtual coupling to allow the passive implementation of a broad class of virtual environments. Section 4.1 provides the most general passivity analysis, with an arbitrary linear two-port virtual coupling. The primary result is a derivation of the conditions under which a haptic display will be passive given any linear two-port virtual coupling. Sections 4.2 and 4.3 explore two physically motivated special cases of the general theory. These special cases allow simpler and more useful passivity conditions to be developed. Section 4.2 specifically addresses admittance causality virtual environments, while §4.3 deals with impedance causality.

4.1 Generalized two-port virtual coupling

In this section, we return to the passivity tools developed in (Colgate and Schenkel 1997), extending them to include a general two-port linear virtual coupling. The goal of the analysis is to derive the conditions under which the haptic display will present a passive impedance to the human operator. Figure 4.1 shows a two-port virtual coupling implementation of a 1 DOF haptic display. As in §3.1, haptic display passivity conditions are derived by demonstrating stability when the human operator is replaced by an arbitrary linear time-invariant passive (ALTIP) impedance.

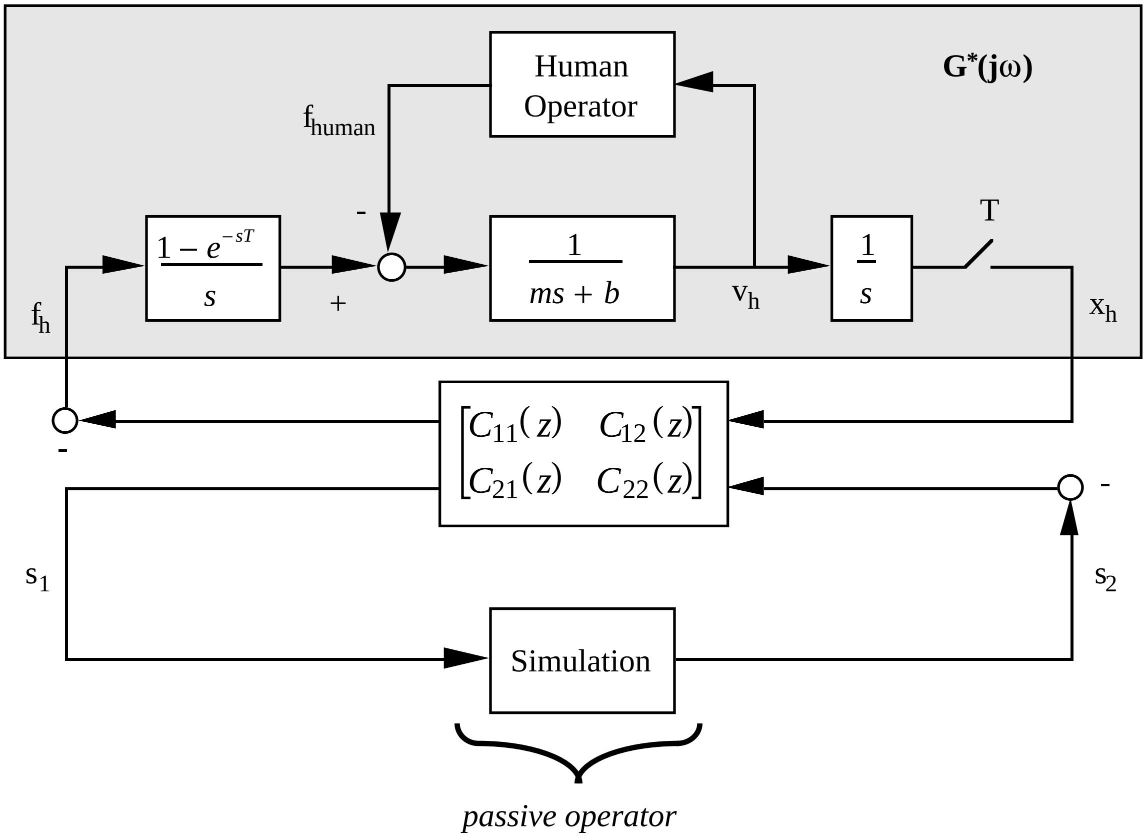

Figure 4.1. Model of a haptic display with a two-port virtual coupling. *G*(jω)* represents the dynamics of the sample/hold, mechanism, and human operator, x_h is the measured position of the haptic display handle, while f_h is the force to be applied to the mechanism by the actuators. Signals s_1 and s_2 are the inputs and outputs of the simulation, and are not required to be specified for the analysis.

The pulse transfer function of the virtual coupling maps x_h and s_2 into f_h and s_1:

(4.1)
$$\begin{bmatrix} -f_h(z) \\ s_1(z) \end{bmatrix} = \begin{bmatrix} C_{11}(z) & C_{12}(z) \\ C_{21}(z) & C_{22}(z) \end{bmatrix} \begin{bmatrix} x_h \\ -s_2 \end{bmatrix}$$

It is assumed that the environment simulation is discrete-time passive (i.e., the mapping from s_1 to s_2 is a passive one according to (2.3) or (2.4)). The model of the continuous portion of the system and the virtual coupling is the same as that used in §3.1. The goal of this analysis is to develop conditions under which the mapping from s_2 to s_1, via the virtual coupling and $G^*(j\omega)$, is a passive one. These conditions will be *sufficient* to establish the stability of the entire system, and *necessary* to establish the passivity of the haptic display.

As in the previous chapter, we model the continuous-time dynamics and the sample-and-hold using the techniques developed in (Colgate and Schenkel 1997). Recall that $G^*(j\omega)$ captures the dynamics of the mechanism, the ALTIP impedance that replaces the human operator, and the sample/hold operators:

$$G^*(j\omega) = \frac{T}{2}\frac{e^{-j\omega T}-1}{1-\cos\omega T}\cdot\frac{1}{mj\omega + b + Z_0(j\omega)} \tag{4.2}$$

where T is the sample time, m is the mechanism inertia, b is the mechanism damping, and $Z_0(j\omega)$ is the ALTIP impedance. The region associated with $G^*(j\omega)$ is a disk whose edge passes through the origin, and whose center and radius are:

$$\text{Center}\left\{G^*(\text{j}\omega)\right\} = \frac{\text{T}}{4\text{b}}\frac{\text{e}^{-\text{j}\omega\text{T}}-1}{1-\cos\omega\text{T}} \tag{4.3}$$

$$\text{Radius}\left\{G^*(\text{j}\omega)\right\} = \frac{\text{T}}{4\text{b}}\left|\frac{\text{e}^{-\text{j}\omega\text{T}}-1}{1-\cos\omega\text{T}}\right| \tag{4.4}$$

Further manipulations can be performed on *$G^*(j\omega)$* through the continued use of Möbius transformations and block diagram manipulation. The transfer function from *$-s_2$* to *s_1* is calculated directly, resulting in the standard coupled stability form shown in Figure 4.2.

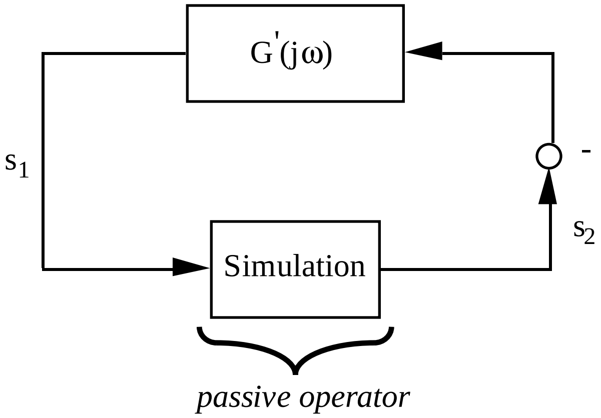

Figure 4.2. Coupled stability form of haptic display system. The mechanism, ALTIP impedance, sample/hold, and two-port virtual coupling dynamics are contained in *$G'(j\omega)$*. The virtual environment is restricted to be discrete time passive.

The mechanism, ALTIP impedance, sample/hold and virtual coupling dynamics are contained in *$G'(j\omega)$*:

(4.5)
$$G'(j\omega) = \left. \frac{-C_{12}(z)\cdot C_{21}(z)\cdot G^*(j\omega)}{1 + C_{11}(z)\cdot G^*(z)} + C_{22}(z) \right|_{z=e^{j\omega T}}$$

The virtual environment is passive, but otherwise arbitrary, so a necessary and sufficient condition for system stability is the strict passivity of *$G'(j\omega)$*. Since *$G'(j\omega)$* is a frequency-dependent region in the complex plane, the Passivity Theorem (2.2) can be used to demonstrate strict passivity:

(4.6) $$\mathrm{Re}\{G'(j\omega)\} > 0$$

Equivalently, the inverse of *G'(jω)* should also have a positive real part:

(4.7) $$Re\left\{\frac{1}{G'(j\omega)}\right\} > 0$$

Substituting (4.5) into (4.6) and (4.7), respectively, yields two equivalent passivity conditions for the haptic display:

(4.8) $$\mathrm{Re}\left\{\frac{-C_{12}(z)\cdot C_{21}(z)\cdot G^{*}(j\omega)}{1+C_{11}(z)\cdot G^{*}(z)} + C_{22}(z)\right\}_{z=e^{j\omega T}} > 0$$

(4.9) $$\mathrm{Re}\left\{\frac{1+C_{11}(z)\cdot G^{*}(z)}{\left[C_{11}(z)\cdot C_{22}(z) - C_{12}(z)\cdot C_{21}(z)\right]\cdot G^{*}(j\omega) + C_{22}(z)}\right\}_{z=e^{j\omega T}} > 0$$

For any given virtual coupling, (4.8) or (4.9) can be evaluated to determine the passivity conditions for the haptic display. The difficulty here is in forming a useful analytic result for the general case. Since *G*(jω)* is a disk in the complex plane, its inverse can be a half-plane, a hole, or another disk, depending on whether *G*(jω)* touches, encompasses, or misses the origin, respectively. Additionally, *G*(jω)* appears in both the numerator and denominator of both (4.8) and (4.9), making it impossible to simplify the results further without specifying something about the virtual coupling.

It is interesting to compare this formulation with that used in (Adams and Hannaford 1998). Adams and Hannaford address the same issues, and in a very similar spirit to the present work. Using a "virtual coupling network", they develop conditions under which a model of a 1 DOF haptic display running a discrete-time passive environment will present a passive impedance to the human operator. The difference between the two formulations is that Adams and Hannaford perform their analysis in discrete time, whereas the present work analyzes the system in continuous time. To analyze a haptic display model in discrete time, both the mechanism and the sample/hold dynamics must be discretized, using any of a variety of techniques. Adams and Hannaford chose Tustin's method to discretize the mechanism dynamics because this method preserves the passivity properties of the operator. They approximated the dynamics of the zero order hold with a digital low-pass filter:

$$\mathrm{ZOH}(z) \cong \frac{1}{2}\left(1 + z^{-1}\right) \tag{4.10}$$

This filter has unity steady-state gain and 90˚ phase lag at the Nyquist frequency. Because their model of the sample-hold process is much simpler than the one used in the present work, broader results were obtained. It is unclear, however, whether the simplified model of sample-hold significantly compromises the accuracy of the results.

The next section considers a physically motivated special case that will allow for more useful results to be obtained.

4.2 Admittance causality virtual environments

Consider the restriction of the virtual environment to admittance causality (i.e., force inputs produce motion outputs). This causality requires s_1 to be a force, since it is the input for the virtual environment. We can further restrict the virtual coupling by requiring it to obey Newton's Third Law, so that the force applied to the haptic display by the actuators is also applied to the virtual environment, but with the opposite sense. With these two restrictions, a one-port representation is adequate to represent the dynamics of the system:

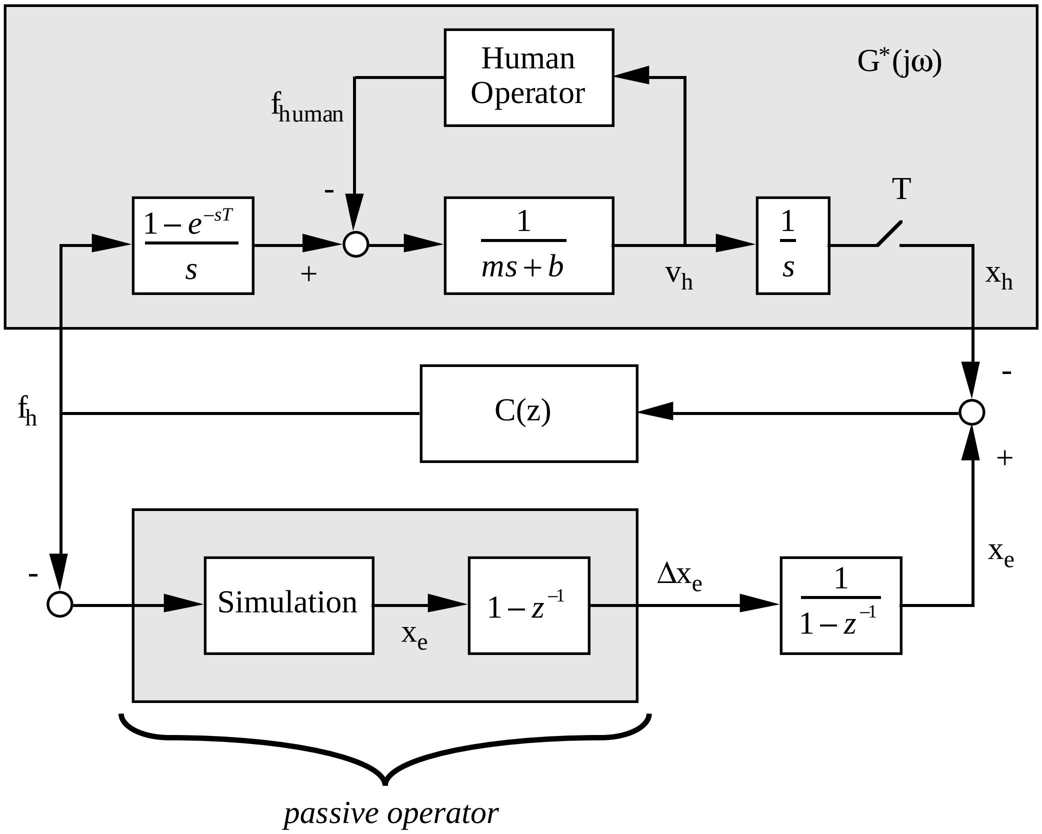

Figure 4.3. Model of a haptic display with a one-port virtual coupling and an admittance causality virtual environment. Note that the simulation outputs position, rather than velocity.

Special care has been taken to use position as the output for the simulation, as the numerical effects of integration are an important part of the passivity/stability characteristics of the system. A more realistic model feeds back both position and velocity, since this approach is typically taken in practice. However, this improved model does not lend itself to a straight forward passivity analysis due to the mismatch in the number of inputs and outputs.

For reasons that will be explained in Chapter 5, passivity conditions for physics-based simulations are developed using force and position change as the inputs and outputs, even though the true output of the simulation is position. The $1\text{-}z^{-1}$ and $1/(1\text{-}z^{-1})$ that follow the simulation are a mathematical construct that permit the analysis to continue, but have no overall effect on the dynamics of the system. Their difference equations are never actually used in the simulation. From this point, the development parallels that of the previous section, as $G^*(j\omega)$ is still given by (3.4). The block diagram now simplifies to the standard coupled stability form shown in Figure 4.4.

The transfer function from Δx_e to f_h and its inverse are calculated directly through block diagram manipulation and Möbius transformations:

$$(4.11)\qquad G^{'}(j\omega) = \left.\frac{f_h(z)}{\Delta x_e(z)}\right|_{z=e^{j\omega T}} = \left.\frac{C(z)}{\left(1-z^{-1}\right)\left[1+C(z)\cdot G^*(j\omega)\right]}\right|_{z=e^{j\omega T}}$$

$$(4.12)\qquad \frac{1}{G^{'}(j\omega)} = \left.\frac{1-z^{-1}}{C(z)} + \left(1-z^{-1}\right)\cdot G^*(j\omega)\right|_{z=e^{j\omega T}}$$

As in the two-port case, a necessary and sufficient condition for system stability is the strict passivity of $G'(j\omega)$. Since $G^*(j\omega)$ is a disk and the Möbius transformations in (4.12)

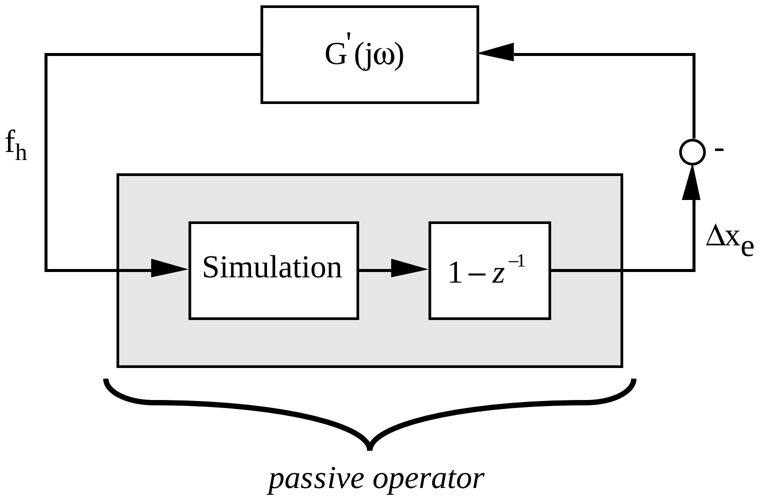

Figure 4.4. Coupled stability form of haptic display system. The mechanism, ALTIP impedance, sample/hold, and one-port virtual coupling dynamics are contained in *G'(jω)*. The virtual environment is restricted to be discrete time passive.

are not inversions, $\frac{1}{G'(j\omega)}$ will also be a disk. The center and radius will be given by c'(jω) and |r'(jω)|, respectively:

$$c'(j\omega) = \frac{T}{2b}\left(\cos\omega T - j\sin\omega T\right) + \frac{1 - e^{-j\omega T}}{C\left(e^{j\omega T}\right)} \tag{4.13}$$

$$\left|r'(j\omega)\right| = \frac{T}{2b} \tag{4.14}$$

In order for *G'(jω)* to be passive, every point in the disk that covers $\frac{1}{G'(j\omega)}$ must have real part greater than zero. In terms of the center and radius, the real part of the center must be greater than the radius:

$$\mathrm{Re}\left\{c'(j\omega)\right\} > \left|r'(j\omega)\right| \tag{4.15}$$

Substituting (4.13) and (4.14) into (4.15), we obtain the conditions under which *G'(jω)* will be passive and the entire haptic display will be guaranteed stable:

$$b > \frac{T}{2}\frac{1-\cos\omega T}{\mathrm{Re}\left\{\dfrac{1-e^{-j\omega T}}{C\left(e^{j\omega T}\right)}\right\}} \tag{4.16}$$

This result is useful because it permits comparison between the effectiveness of different virtual couplings that might be used with admittance causality virtual environments.

As an example, consider the spring and damper coupling implementation mentioned previously, whose continuous-time transfer function is given by:

$$C(s) = K + Bs \tag{4.17}$$

where *K* and *B* are the virtual stiffness and damping. The discrete version of this transfer function depends on the mapping used between continuous and discrete time and on the sample time *T*. For example, we can calculate the discrete-time transfer functions for a backwards difference and Tustin's mapping, respectively:

$$C_{BD}(z) = K + \frac{B}{T}\left(1-z^{-1}\right) \tag{4.18}$$

$$C_{Tustin}(z) = K + \frac{2B}{T}\left(\frac{1-z^{-1}}{1+z^{-1}}\right) \tag{4.19}$$

Substitution of (4.17) and (4.18) into (4.15) yields two different passivity conditions for the two different virtual couplings. For the spring/damper using the backwards difference, the passivity condition for the haptic display is the same as that found previously:

$$b > \frac{KT}{2} + B \tag{4.20}$$

This result indicates that for a given mechanism damping level and simulation update rate, the virtual stiffness and damping of the coupling can be chosen such that *any* discrete-time passive simulation will meet necessary conditions for device passivity. The simulation can be based on any physics-based modeling technique, whether linear or non-linear, as long as it obeys discrete-time passivity. By comparison, the passivity condition for the spring/damper using Tustin's mapping is:

$$b > \left(\frac{KT}{2} + B\right)\frac{1 + 2\lambda\cos\omega T + \lambda^2}{2(1 + \cos\omega T)(1 + 2\lambda\cos\omega T)} \qquad \lambda = \frac{KT - 2B}{KT + 2B} \tag{4.21}$$

This expression indicates that infinite physical damping is necessary at the Nyquist frequency, making (4.19) a poor candidate for a virtual coupling for certain passive virtual environments. Optimization of the virtual coupling is the subject of current and future work. To date, however, no published works have documented significantly improved performance over the backwards difference spring-damper virtual coupling mentioned above.

4.3 Impedance causality virtual environments

In this section, we consider the restriction of the virtual environment to impedance causality (i.e., motion inputs produce force outputs). While probably not the optimal formulation for multibody systems, impedance environments have been used in many simulations. Adams and Hannaford (Adams, et al. 1998) showed that any virtual coupling used with admittance environments can be used with impedance environments as well, albeit with a slightly different implementation in software.

Returning to the two-port structure of Figure 4.1, this causality requires s_2 to be a force, since it is the output of the virtual environment. As in the previous section, we can further restrict the virtual coupling by requiring it to obey Newton's Third Law, so that the virtual environment's output force is sent directly to the haptic display's actuators, but with the opposite sense. With these restrictions, a one-port representation is adequate to represent the dynamics of the system.

As in the admittance causality case, the $1\text{-}z^{-1}$ and $1/(1\text{-}z^{-1})$ operators are a mathematical construct and are not implemented in actual simulations. The transfer function from $-f_e$ to Δx_e (via the virtual coupling and $G^*(j\omega)$) is calculated directly through block diagram manipulation:

(4.22) $$G^{'}(j\omega) = \left.\frac{\Delta x_e(z)}{-f_e(z)}\right|_{z=e^{j\omega T}} = \left.\left(1-z^{-1}\right)\cdot G^*(j\omega) + \frac{1-z^{-1}}{C(z)}\right|_{z=e^{j\omega T}}$$

which is the inverse of $G'(j\omega)$ in the admittance case.

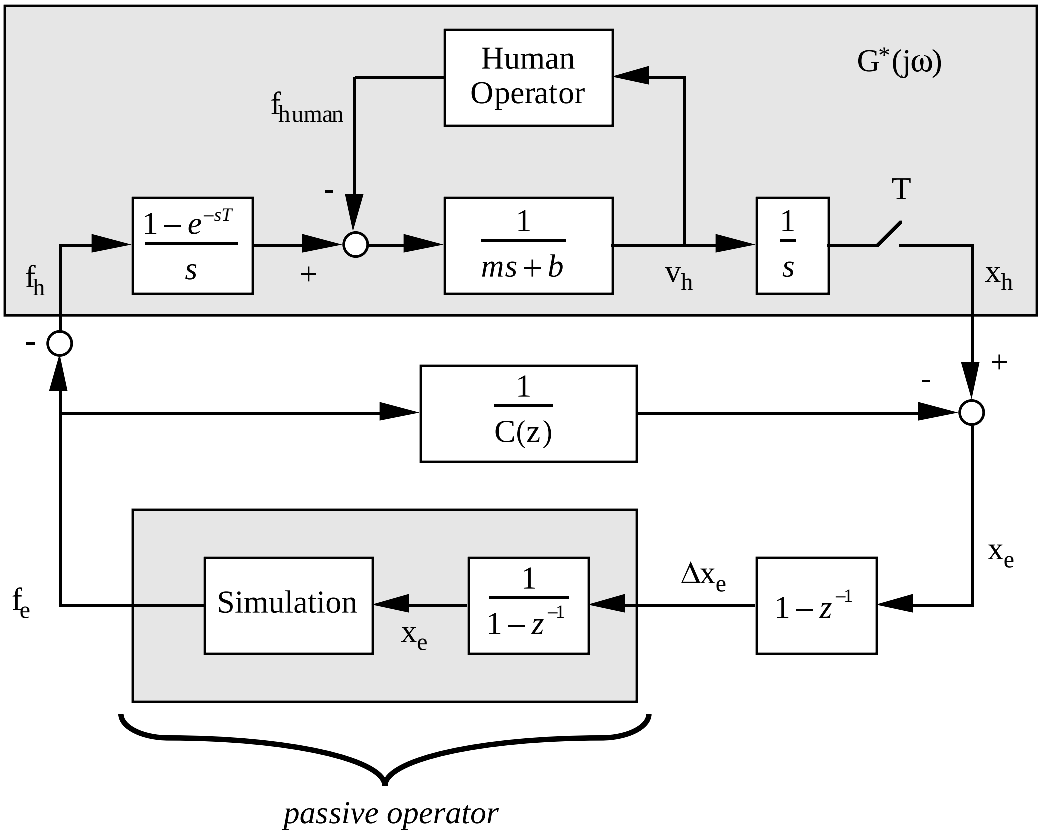

Figure 4.5. Impedance causality virtual environment with one-port virtual coupling. The virtual coupling, *C(z)*, is the same as that used for admittance environments.

As a result, the passivity conditions remain the same as in the admittance case.

$$b > \frac{T}{2}\frac{1-\cos\omega T}{\mathrm{Re}\left\{\frac{1-e^{-j\omega T}}{C\left(e^{j\omega T}\right)}\right\}} \tag{4.23}$$

As in the previous case, this result is helpful because it permits comparison between the effectiveness of different virtual couplings that might be used with impedance causality virtual environments. The remainder of the document, however, will focus on admittance causality virtual environments because they seem to be better suited for multibody simulations.

The use of a virtual coupling like the backwards-difference damped spring allows the designer to focus on multibody simulation rather than sampled-data stability issues. The only requirement, from a passivity point of view, is that the numerical methods in the simulation be discrete-time passive. This change in focus is desirable because discrete-time passivity has a meaningful interpretation when dealing with physics-based numerical methods. The next chapter explores this issue in greater depth.

CHAPTER 5

DISCRETE-TIME PASSIVITY OF PHYSICS-BASED NUMERICAL METHODS

In the analyses of the previous two chapters, it was assumed, without explanation, that the simulation obeys the property of *discrete-time passivity*. This chapter investigates the connection between discrete-time passivity and the conservation properties of the numerical methods used in multibody simulations. The general contribution of the chapter is to show that if a numerical method meets a specific energy conservation guideline, it will be discrete-time passive. This result establishes, in the context of physics-based simulations, guidelines for numerical operators so that they can then be used with a properly designed virtual coupling to create extremely robust multibody simulations for haptic display.

Admittance causality physics-based simulations begin with a force input (in this case from the virtual coupling). From this point, a multibody simulation consists of five distinct modules: bilateral constraint formulation, integration, collision detection, contact point determination, and collision response. These modules are together responsible for advancing the state of the simulation through time and computing the forces that are fed back to the human operator through the virtual coupling and haptic display hardware. They must be able to enforce constraints, detect collisions between bodies, and respond to them in a physically meaningful manner.

For even moderately complicated environments, the most computationally intensive module is collision detection, and improving the efficiency of these algorithms is currently an extremely active area of research (for a survey, see (Lin and Gottschalk 1998)). However, it will suffice for this document to say that collision detection should be as fast as possible, because computational delay tends to compromise passivity. For additional detail regarding collision detection and contact point determination for haptic display, see (Chang 1998).

The subtleties of numerical integration and collision response, however, merit closer investigation. Their effect on discrete-time passivity can be quite pronounced, even though they are not a severe computational burden compared to collision detection. §5.1 discusses in general terms the different methods for evaluating the performance of numerical integrators used in real-time simulations for haptic display. §5.2 presents the most general result, an incremental energy conservation principle that guarantees discrete-time passivity of numerical operators. This conservation principle can be applied to any physics-based numerical method, regardless of the types of models used in the environment. §5.3 explores a simple example, a particle constrained to a line. It is shown that the conservation principle of the previous section has a meaningful physical interpretation, and can be used to design discrete-time passive numerical integrators. §5.4 and §5.5 extend the analysis to a particle in a plane and a rigid body in space, respectively, while §5.6 further extends the results to include collision models between rigid bodies.

5.1 Performance evaluation for physics-based numerical methods

When modeling complex dynamic systems, the result is typically a set of non-linear differential equations with no known analytic solution. Often, researchers must resort to using a numerical method to approximate the solution to this set of equations. There is no "best" way to approach this task in general, and a vast research literature has developed which explores different approaches for a wide variety of applications. In our case, we are interested in obtaining solutions to sets of ordinary differential equations that represent the dynamics of rigid-body mechanical systems. As in the general case, there are no clear "best" ways of obtaining solutions. However, several different measures of numerical method "goodness" have developed over the years:

1) **Accuracy** -- Use the numerical method to simulate a set of equations to which there is a known analytic solution, and compare the numerical result to the analytic one. If the error is within some threshold set by the analyst, then the numerical method is judged to be "good enough."

2) **Stability** -- Some numerical methods have the potential to become numerically unstable when it is known that the true solution does not. Obviously, if this situation arises, the numerical method has failed.

3) **Conservation properties** -- In many cases, while the solution itself is unknown, it is known that the solution must obey certain overriding physical principles, such as conservation of momentum or energy. If these conservation principles are met within some threshold set by the analyst, the numerical method is judged to be "good enough."

4) **Computational efficiency** -- In many cases, particularly when dealing with simulations that must run in real time, computational efficiency can become an overriding

factor in evaluating performance. Frequently, methods that are accurate, stable and observe the relevant conservation properties fail because they take too long to execute. For successful real time operation, the analyst needs to provide a guarantee that the numerical method will yield a solution within a given period of time.

The remainder of the chapter focuses on stability, conservation properties, and computational efficiency. However, while computational efficiency is important, and any algorithms will need to be realizable in real time, the primary concern in this chapter is to understand the "right" way of implementing rigid-body dynamic simulations for haptic display.

5.2 Incremental discrete-time passivity

For an arbitrary operator *G* with input *u* and output *y*, recall the basic definition for discrete-time passivity:

$$\sum_{k=0}^{N} u_k \cdot y_k \geq -E_0 \qquad \forall\ u_k, \forall\ N \in \mathbb{Z}^+ \tag{2.3}$$

where E_0 is a constant dependent on the internal initial conditions of the dynamic operator *G*. This expression is difficult to evaluate for physics-based simulation methods because it requires evaluation for all possible input trajectories over all time. In this section, we demonstrate an incremental condition that, given some simple restrictions on the operator, provides a guarantee that the numerical method will be discrete-time passive. An incremental condition is easier to use because it is does not require evaluation of entire trajectories over time, but rather represents a restriction on the updated state based only on the current state and the most recent input.

The operator *G* represents the dynamics of a physics-based simulation, so it can be non-linear and may have any number of internal states in addition to the input and output. However, if the following two conditions are met at each step, then *G* will be discrete-time passive:

1) Operator *G* has an energy storage function, *E*, that is based solely on the internal state of the simulation at a given step and is bounded from below by E_{min}.
2) For any internal state at step *k-1* (with stored energy E_{k-1}) and input u_k, the algorithm meets the following restriction on y_k and E_k:

$$u_k y_k \geq E_k - E_{k-1} \tag{5.1}$$

To see that these conditions result in a discrete-time passive method, consider the summation over all steps:

$$\begin{aligned}
\sum_{k=1}^{N} u_k y_k &\geq \sum_{k=1}^{N} \left(E_k - E_{k-1}\right) \\
&\geq \left(E_1 - E_0\right) + \left(E_2 - E_1\right) + \left(E_3 - E_2\right) + \cdots + \left(E_N - E_{N-1}\right) \\
&\geq E_N - E_0 \\
&\geq \left(E_N - E_{min}\right) + E_{min} - E_0 \qquad (5.2)
\end{aligned}$$

Since *(E_N-E_{min})* must be non-negative, the operator must be discrete-time passive:

(5.3)
$$\sum_{k=1}^{N} u_k y_k \geq E_{min} - E_0$$

Equation (5.1) can be interpreted as an incremental energy conservation principle, such that any extracted work must at least be matched by an equal drop in the internal energy stored in the system. The result implies that *any* numerical operator, linear or non-linear, that observes a conservation principle like that of (5.1) will result in a passive mapping from input to output. In the following sections, this principle will be applied to various examples and used as a design tool for physics-based numerical methods.

5.3 Discrete-time passive numerical integration of a 1 DOF particle

Consider a particle *P*, constrained to move along a line, with a time-varying force acting on it, as shown in Figure 5.1.

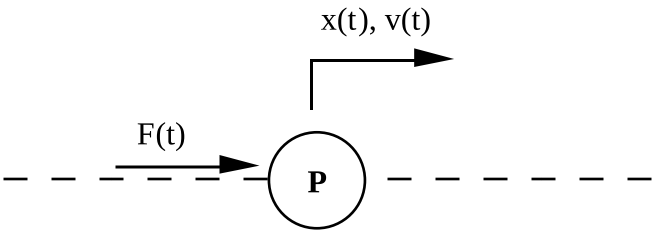

Figure 5.1. Particle constrained to a line. The particle has mass *m*, with force *F(t)* acting on it.

The equation of motion for this system is:

(5.4) $$\ddot{x} = \frac{F(t)}{m}$$

The analytic solution to this second-order differential equation can be obtained directly if *F(t)* is integrable:

(5.5) $$\mathrm{v}(\mathrm{t}) = \mathrm{v}(\mathrm{t}_0) + \frac{1}{\mathrm{m}}\int_{\mathrm{t}_0}^{\mathrm{t}} \mathrm{F}(\mathrm{t})\mathrm{dt} \qquad \forall \mathrm{t} \geq \mathrm{t}_0$$

(5.6) $$\mathrm{x}(\mathrm{t}) = \mathrm{x}(\mathrm{t}_0) + \int_{\mathrm{t}_0}^{\mathrm{t}} \mathrm{v}(\mathrm{t})\mathrm{dt} \qquad \forall \mathrm{t} \geq \mathrm{t}_0$$

with the following initial conditions:

(5.7) $$v(t_0)=v_0 \qquad x(\mathrm{t}_0)=x_0$$

It should be noted that this system inherently obeys two conservation laws: conservation of momentum and conservation of energy.* The time integral form of (5.4) expresses the momentum balance for this system:

(5.8) $$mv(t) - mv_0 = \int_{t_0}^{t} F(t)dt$$

* In many texts, "conservation of energy" is closely tied to systems with conservative forces. In this document, conservation of energy means that the change in kinetic energy equals the sum of work done by external forces.

The change in momentum exactly equals the total impulse applied by the external force over any time period. The energy balance for the system can be obtained by expressing the power flow into the system and then integrating with respect to time.

(5.9)
$$\begin{aligned}\int_{t_0}^{t} F(t)v(t)dt &= \int_{t_0}^{t} m\dot{v}(t)v(t)dt \\ &= \frac{1}{2}mv^2 - \frac{1}{2}mv_0^2\end{aligned}$$

The work done by the external force exactly equals the change in kinetic energy of the mass. We will see that, even for this simple example, numerical integration methods do not necessarily yield solutions that observe these basic conservation laws of mechanical systems. It is these conservation laws that will be used later in the section to form incremental passivity conditions for numerical integrators.

One approach to numerical approximation begins by breaking the single second-order differential equation into two first order differential equations:

(5.10)
$$\begin{bmatrix}\dot{v}(t)\\ \dot{x}(t)\end{bmatrix} = \begin{bmatrix}0 & 0\\ 1 & 0\end{bmatrix}\begin{bmatrix}v(t)\\ x(t)\end{bmatrix} + \begin{bmatrix}F(t)/m\\ 0\end{bmatrix}$$

Now the equations of motion are in a form more amenable to standard numerical integration techniques. Possibly the simplest numerical integration scheme is the Euler method:

(5.11)
$$\begin{bmatrix}v_k\\ x_k\end{bmatrix} = \begin{bmatrix}1 & 0\\ T & 1\end{bmatrix}\begin{bmatrix}v_{k-1}\\ x_{k-1}\end{bmatrix} + \begin{bmatrix}f_{k-1}T/m\\ 0\end{bmatrix}$$

As done above for the analytic solutions, we can formulate the momentum and energy balances for this system. It is important to remember, however, that these conservation laws are somewhat arbitrary when discussed in discrete time. This arbitrariness arises because both (5.8) and (5.9) involve time integrals of continuous time signals. For example, the top half of (5.11) can be used to compare the total impulse applied by the external force with the momentum change of the mass. While the change in momentum is well defined from step *k-1* to *k*, calculating the total impulse requires an estimation of the force that acts to produce the change in momentum. It seems to make sense, however, to use the same force estimation as used by the integrator itself. For Euler integration, the momentum balance becomes:

$$f_{k-1}T = mv_k - mv_{k-1} \tag{5.12}$$

It is easy to see that the change in momentum of the mass exactly equals the total impulse applied by the external force. Similarly, both parts of (5.11) can be used to compare the work done by the force from step *k-1* to *k* with the kinetic energy change of the mass:

$$\begin{aligned} W_{k-1:k} &= f_{k-1} \cdot (x_k - x_{k-1}) \\ &= mv_k v_{k-1} - mv_{k-1}^2 \\ &\neq \frac{1}{2}mv_k^2 - \frac{1}{2}mv_{k-1}^2 \end{aligned} \tag{5.13}$$

where the force estimate from time t_{k-1} to t_k is f_{k-1}. Here we can clearly see that the change in kinetic energy of the mass in fact does *not* exactly equal the work done by the external force. Figure 5.2 shows the energy balance for this particular numerical integrator with a sinusoidal input force. It is easy to see that mass is receiving more energy than the external force is giving to it.

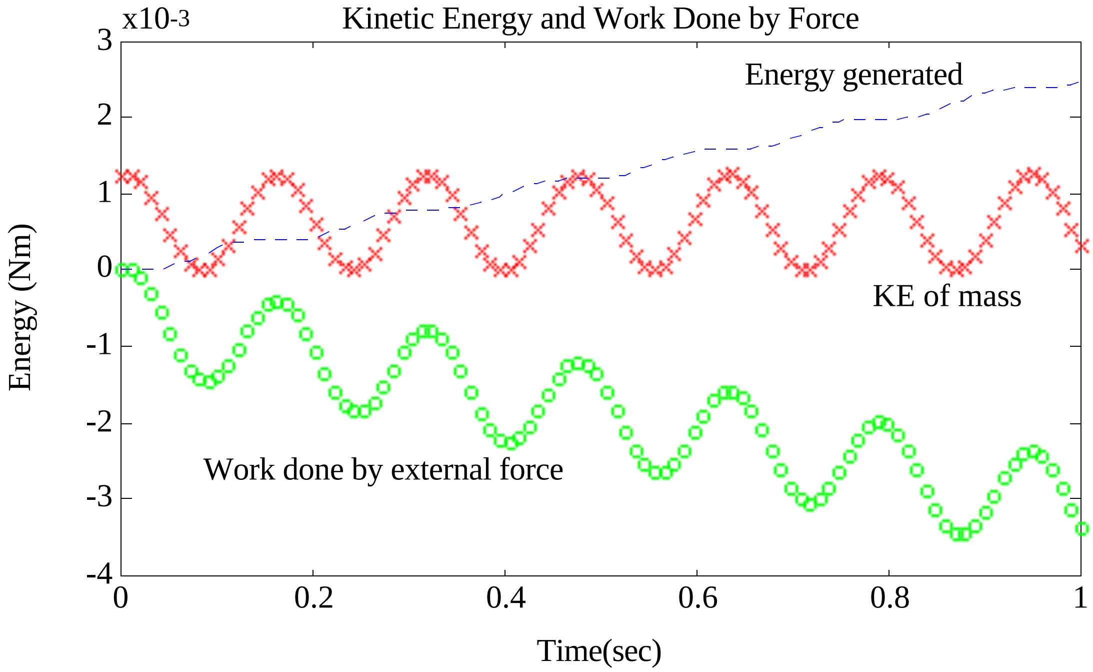

Figure 5.2. Energy balance for the Euler integration of a particle with a sinusoidal input force.

Having established that some numerical integrators do not yield results that are consistent with overriding conservation principles of mechanical systems, we are faced with the more daunting task of finding or designing a numerical integrator that does obey them. For the 1 DOF particle, it becomes quite straight forward to design the integrator from first principles. The momentum balance (5.12) determines how the velocity is updated, while the energy balance (5.14) determines how position is updated:

$$f_{k-1}(x_k - x_{k-1}) = \frac{1}{2}mv_k^2 - \frac{1}{2}mv_{k-1}^2 \tag{5.14}$$

Solving (5.12) and (5.14) for v_k and x_k yields the update equations for the numerical integrator, which is a first order Taylor series integrator (Euler method) for the velocity update and a second order Taylor series integrator for position update:

$$\begin{bmatrix} v_k \\ x_k \end{bmatrix} = \begin{bmatrix} 1 & 0 \\ T & 1 \end{bmatrix} \begin{bmatrix} v_{k-1} \\ x_{k-1} \end{bmatrix} + \begin{bmatrix} 2 \\ T \end{bmatrix} \frac{f_{k-1}T}{2m} \tag{5.15}$$

Figure 5.3 shows the energy balance for a sample integration using this numerical integration scheme. Clearly, energy is conserved for this system.

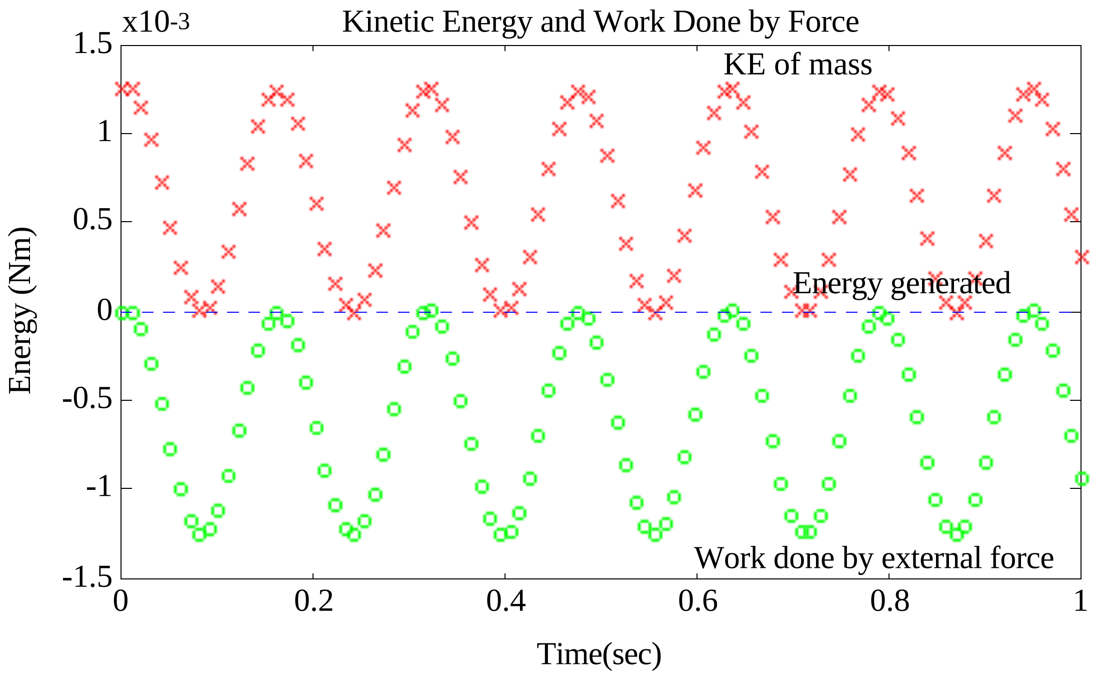

Figure 5.3. Energy balance for the energy-conserving integration of a particle with a sinusoidal input force.

We could have used a different estimation of force from t_{k-1} to t_k, which would have resulted in a different approximation for work. As long as the resulting definition of work is used to form the integrator, it will conserve energy according to that particular definition.

The importance of energy conserving integrators relates to the incremental passivity conditions developed in the previous section. In the following development, we show how a numerical integrator can obey (5.1), and in turn, how the operator from force to position change is a passive one. Consider the non-delayed* version of the energy/momentum conserving integrator examined previously:

$$\begin{bmatrix} v_k \\ x_k \end{bmatrix} = \begin{bmatrix} 1 & 0 \\ T & 1 \end{bmatrix} \begin{bmatrix} v_{k-1} \\ x_{k-1} \end{bmatrix} + \begin{bmatrix} 2 \\ T \end{bmatrix} \frac{f_k T}{2m} \tag{5.16}$$

The energy balance for this integrator differs from (5.14) only in the subscript on force:

$$f_k(x_k - x_{k-1}) = \frac{1}{2} m v_k^2 - \frac{1}{2} m v_{k-1}^2 \tag{5.17}$$

The first requirement of incremental passivity is the existence of an internal energy storage function that is bounded from below. In this case, the kinetic energy of the mass meets this condition because it must be non-negative. The second requirement of incremental passivity is given by (5.1), which places a restriction on how the state is updated at each step. Comparison between (5.17) with (5.1) demonstrates that the first order/second order Taylor integrator is discrete-time passive in the mapping between

* This difference equation is "non-delayed" because x_k and v_k depend on f_k. They depend on f_{k-1} in the previous example, making the integrator of (5.11) "delayed". This issue will be revisited in Chapter 6.

force and position change. The passivity developments of the previous chapter imply that because it is discrete-time passive, this integrator should be extremely robust when used with a virtual coupling architecture.

5.4 Discrete-time passive numerical integration of a 2 DOF particle

Before exploring the dynamics of a rigid body in space, let us consider extending the results of the previous section to higher degrees of freedom, but without the complexity of three-dimensional rotations. For example, suppose the particle in the previous example was not constrained to travel on a line, but instead allowed to travel in a plane (Figure 5.4).

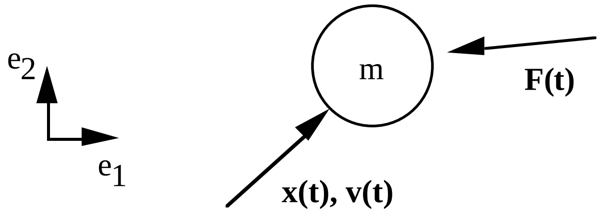

Figure 5.4. Two DOF particle, with position **x(t)** and velocity **v(t)**, and an arbitrary force **F(t)** acting on it (note that **x(t)**, **v(t)** and **F(t)** are all vectors).

In vector form, the equations of motion for this system are:

$$\mathbf{F(t)} = \mathbf{M\ddot{x}(t)} \tag{5.18}$$

where **M** is a constant mass matrix:

(5.19)
$$\mathbf{M} = \begin{bmatrix} m & 0 \\ 0 & m \end{bmatrix}$$

Conservation of momentum and energy expressions can be obtained using the same techniques as in the previous section:

(5.20)
$$\int_{t_0}^{t} F_i(t)dt = mv_i(t) - mv_i(t_0) \qquad i=1,2$$

(5.21)
$$\begin{aligned} \int_{t_0}^{t} F_i(t)v_i(t)dt &= \int_{t_0}^{t} m\dot{v}_i(t)v_i(t)dt \\ &= \frac{1}{2}mv_i^2 - \frac{1}{2}mv_{i,0}^2 \end{aligned} \qquad i=1,2$$

Clearly, the analytic solution will obey momentum and energy conservation principles. As in the 1 DOF case, we would like to use these conservation properties to design a numerical integrator that is discrete-time passive. For the 2 DOF system, there are four difference equations that need to be updated at each step (2 positions and 2 velocities):

(5.22)
$$\begin{bmatrix} \mathbf{v_k} \\ \mathbf{x_k} \end{bmatrix} = g\left(\begin{bmatrix} \mathbf{v_{k-1}} \\ \mathbf{x_{k-1}} \end{bmatrix}, \mathbf{f_k}\right)$$

where *g(·)* is some function representing the numerical integrator. There are also four constraint equations that must be met (2 for momentum and 2 for energy):

$$f_{i,k}T = m(v_{i,k} - v_{i,k-1}) \qquad i=1,2 \tag{5.23}$$

$$f_{i,k}(x_{i,k} - x_{i,k-1}) = \frac{1}{2}mv_{i,k}^2 - \frac{1}{2}mv_{i,k-1}^2 \qquad i=1,2 \tag{5.24}$$

As in the 1 DOF case, we can solve the constraints algebraically to obtain the difference equations that can be used for integration:

$$\begin{bmatrix} v_{i,k} \\ x_{i,k} \end{bmatrix} = \begin{bmatrix} 1 & 0 \\ T & 1 \end{bmatrix} \begin{bmatrix} v_{i,k-1} \\ x_{i,k-1} \end{bmatrix} + \begin{bmatrix} 2 \\ T \end{bmatrix} \frac{f_{i,k}T}{2m} \qquad i=1,2 \tag{5.25}$$

Let us compare the number of dynamic equations with the number of "constraint" equations for both the 1 DOF and the 2 DOF cases. For the 1 DOF system, there are two difference equations that need to be updated each step (one for position and one for velocity) and two constraint equations (1 for momentum, 1 for energy). Thus, the algorithm is completely constrained, indicating that (5.16) is the only numerical integrator that exactly conserves both momentum and energy for the 1 DOF particle (of course, other more complicated methods may simplify to this result for such a simple system). In the 2 DOF case, there are four update equations and four independent constraint equations, specifying the update procedure entirely.

At this point, we must make a clarification that will become important when dealing with 3-dimensional rotations. Strictly speaking, there should be only one energy conservation equation, rather than the two of (5.24). In fact, true energy conservation for this example would be met by summing (5.24) over all degrees of freedom:

$$\int_{t_0}^{t} F_1 v_1 dt + \int_{t_0}^{t} F_2 v_2 dt = \frac{1}{2}mv_1^2 - \frac{1}{2}mv_{1,0}^2 + \frac{1}{2}mv_2^2 - \frac{1}{2}mv_{2,0}^2 \qquad (5.26)$$

A better name for the principle that is enforced by (5.24) is *conservation of work*. Any work done by external forces can show up only in certain types of motions, as determined by the component form of the energy/work equations. For this specific example, the equations of motion indicate that the degrees of freedom can be completely separated from one another, making it seem as if there is conservation of energy within each degree of freedom. We will see that for a rigid body rotating in space, however, the degrees of freedom are coupled, making the work conservation equations coupled as well.

5.5 Discrete-time passive numerical integration of a rigid body in space

This section demonstrates the difficulties encountered when attempting to generalize the numerical integrator design approach outlined in the previous two sections. Consider a single rigid body β in 3-dimensional space with a time-varying force acting upon it, as shown below in Figure 5.5. Any externally applied force **F**(t) can be equivalently modeled as a force $\mathbf{F_e}$(t) at the center of mass and an externally applied torque $\mathbf{N_e}$(t) as shown in Figure 5.6.

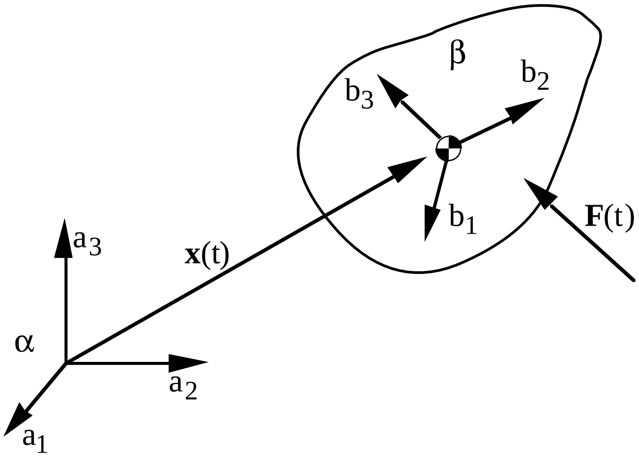

Figure 5.5. Rigid body β moving in inertial frame α. Vector **x**(t) describes the location of the mass center with respect to a fixed point in α. Local coordinate system **b** is fixed in the body frame, and is aligned with the principle axes of β. The orthogonal transformation Λ(t) defines the orientation of **b** with respect to α-fixed **a**. **F**(t) is an external force acting on body β.

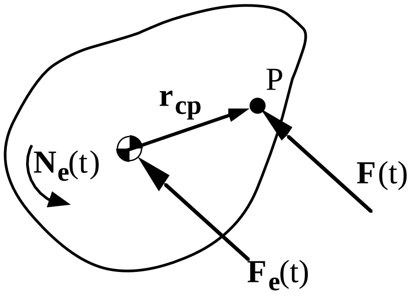

Figure 5.6. Equivalent force/torque pair. Force **F(t)** is applied at point *P*, whereas **Fe(t)** is applied to the center of mass, with an external torque **Ne(t)** also applied to the body.

The equivalent force and torque are given by:

$$\mathbf{F}_\mathbf{e}(t) = \mathbf{F}(t) \qquad \mathbf{N}_\mathbf{e}(t) = \mathbf{r}_\mathbf{CP} \times \mathbf{F}(t) \tag{5.27}$$

where $\mathbf{r_{cp}}$ is a vector pointing from the center of mass to the point of application of the external force. Thus, without loss of generality, we will consider only forces applied to the center of mass, and we will drop the subscripts indicating that the force (or torque) is part of an equivalent force/torque. The equations of motion for this system are given in terms of the linear momentum, **p**, and the angular momentum, **L**, about the center of mass.

(5.28) $$\mathbf{F}(t) = \frac{d\mathbf{p}}{dt} \qquad \mathbf{N}(t) = \frac{d\mathbf{L}}{dt}$$

The linear momentum for a rigid body is expressed using the total mass *m* and the velocity $\mathbf{v_c}$ of the mass center, while angular momentum about the mass center uses the inertia dyadic **I** and angular velocity ω of the body:

(5.29) $$\mathbf{p}(t) = m\mathbf{v_c}(t)$$

(5.30) $$\mathbf{L}(\mathrm{t}) = \mathbf{I}\omega(\mathrm{t})$$

Time integration of (5.28) yields the momentum conservation equations for this system:

(5.31) $$\int_{t_0}^{t} \mathbf{F}(t)dt = \mathbf{p}(t) - \mathbf{p_0} \qquad \int_{t_0}^{t} \mathbf{N}(t)dt = \mathbf{L}(t) - \mathbf{L_0}$$

where $\mathbf{p_0}$ and $\mathbf{L_0}$ are the initial linear and angular momentum, respectively. The work conservation equations can be best understood by writing (5.28) in component form:

$$(5.32) \qquad F_i = \frac{dp_i}{dt} \qquad N_i = \frac{dL_i}{dt} \qquad i\text{=1,2,3}$$

Post-multiplication of $(5.32)_1$ by v_i and integration with respect to time yields the work conservation equations for the translational portion of the system:

$$(5.33) \qquad \int_{t_0}^{t} F_i(t)\cdot v_i(t)dt = \frac{1}{2}mv_i^2(t) - \frac{1}{2}mv_{i,0}^2 \qquad i\text{=1,2,3}$$

As in the example of the particle in a plane, independent conservation equations can be written for each translational degree of freedom. The rotational portion, however, does not share this property. The easiest way to see this effect is to express the rotational equations of motion in body coordinates (**b**). Because the time derivative of momentum must be calculated with respect to the inertial frame, $(5.28)_2$ becomes:

$$(5.34) \qquad \mathbf{N}(t) = \left(\frac{d\mathbf{L}}{dt}\right)_{\beta} + \omega \times \mathbf{L}$$

Since the body coordinates are aligned with the principle axes, (5.34) can be expanded to a fairly simple form, commonly known as *Euler's equations of motion* for a rigid body with one point fixed (for a full derivation, see (Goldstein 1980)):

$$(5.35) \qquad \begin{aligned} N_1 &= I_1\dot{\omega}_1 - \omega_2\omega_3(I_2 - I_3) \\ N_2 &= I_2\dot{\omega}_2 - \omega_3\omega_1(I_3 - I_1) \\ N_3 &= I_3\dot{\omega}_3 - \omega_1\omega_2(I_1 - I_2) \end{aligned}$$

where I_i are the principle moments of inertia of body β. Post-multiplication by ω_i and integration with respect to time yields the work conservation equations for the rotational portion of the system:

$$\begin{aligned}
\int_{t_0}^{t} N_1\omega_1 dt &= \frac{1}{2}I_1\omega_1^2 - \frac{1}{2}I_1\omega_{1,0}^2 - \int_{t_0}^{t} \omega_2\omega_3(I_2 - I_3)\omega_1 dt \\
\int_{t_0}^{t} N_2\omega_2 dt &= \frac{1}{2}I_2\omega_2^2 - \frac{1}{2}I_2\omega_{2,0}^2 - \int_{t_0}^{t} \omega_3\omega_1(I_3 - I_1)\omega_2 dt \\
\int_{t_0}^{t} N_3\omega_3 dt &= \frac{1}{2}I_3\omega_3^2 - \frac{1}{2}I_3\omega_{3,0}^2 - \int_{t_0}^{t} \omega_1\omega_2(I_1 - I_2)\omega_3 dt
\end{aligned} \tag{5.36}$$

These results demonstrate that the energy/work equations for three-dimensional rigid-body rotation are coupled. Individual axes of rotation do not in fact observe conservation of work. The sum of the above equations shows, however, that the work done by the external force exactly equals the change in kinetic energy of the body.

$$\begin{aligned}
\int_{t_0}^{t} \left(N_1\omega_1 + N_2\omega_2 + N_3\omega_3\right)dt &= \int_{t_0}^{t} \left(I_1\dot{\omega}_1\omega_1 + I_2\dot{\omega}_2\omega_2 + I_3\dot{\omega}_3\omega_3\right)dt \\
&= \sum_{i=1}^{3}\frac{1}{2}I_i\omega_i^2 - \sum_{i=1}^{3}\frac{1}{2}I_i\omega_{i,0}^2
\end{aligned} \tag{5.37}$$

As in the previous two sections, we would like to design a numerical integrator for this system that inherently preserves these overriding properties, resulting in an integrator that obeys incremental discrete-time passivity. Since a single rigid body has six degrees of freedom, there are twelve update equations to specify. Conservation of momentum yields six constraint equations and conservation of work yields six more. Unlike the previous cases, though, these constraints are highly coupled and some of the terms are non-integrable, so a complete solution remains to be found. The translational portion can be addressed via the method outlined in §5.2, yielding six translational update equations that meet conservation of linear momentum/work:

$$\begin{bmatrix} v_{i,k} \\ x_{i,k} \end{bmatrix} = \begin{bmatrix} 1 & 0 \\ T & 1 \end{bmatrix} \begin{bmatrix} v_{i,k-1} \\ x_{i,k-1} \end{bmatrix} + \begin{bmatrix} 2 \\ T \end{bmatrix} \frac{f_{i,k}T}{2m} \qquad i=1,2,3 \tag{5.38}$$

For the rotational portion of the system, discrete momentum equations can be developed using $(5.31)_2$:

$$\mathbf{N_k}T = \mathbf{L_k} - \mathbf{L_{k-1}} \tag{5.39}$$

These constraint equations are more difficult to meet than in the translational case because the angular momentum depends on both angular velocity and orientation (as opposed to velocity alone in the translational case). Simo (Simo and Wong 1991) successfully implements this constraint by forming (5.39) in body coordinates:

$$\Lambda_k \mathbf{I}\omega_k - \Lambda_{k-1}\mathbf{I}\omega_{k-1} = T\overline{\mathbf{N}}_{k-1+\alpha} \tag{5.40}$$

where $\overline{\mathbf{N}}_{k-1+\alpha}$ is an estimation of applied torque over the time step (for passivity purposes, we will use $\alpha=1$) and Λ_k is the orientation of the body with respect to the inertial frame.

Because of the form of (5.34), discrete conservation of work is significantly more difficult to enforce than discrete momentum conservation. While $(5.31)_2$ can be integrated analytically to obtain (5.39), some terms in (5.36) are non-integrable, making it unclear how best to proceed. Conservation of energy can be enforced using (5.37), yielding one constraint equation. While sufficient to establish discrete-time passivity of the map from torque to angle of rotation, a method that obeys a discrete version of (5.36) should in theory be more accurate. There are several integrator candidates that are energy conserving for force-free motions (LaBudde and Greenspan 1976, Sasaki 1976, Simo and Wong 1991), but it remains to be seen whether they obey conservation of energy or some form of conservation of work. These properties will be necessary to ensure discrete-time passivity of the numerical method.

The previous two sections have addressed the significance of incremental discrete-time passivity for numerical integrators. The most important point to understand is that if a numerical integrator is energy conserving in the sense of (5.1) it will be discrete-time passive over all possible input trajectories. Further, it is straight forward to design integrators with this property for translations, but not for three dimensional rotations.

5.6 Discrete-time passive collision response

After integration and collision detection, the final component of a multibody simulation is constraint enforcement. In this document, we will focus on unilateral constraints, which occur whenever bodies collide. They resist the interpenetration of bodies, but do not hold them together. Unilateral constraints are one of the most noteworthy features of interaction, and one of the most troublesome for haptic display. Bilateral constraints, such as revolute and prismatic joints, are also important for multibody simulation. However, the complexity they introduce to integration and collision response algorithms is such that they remain a topic for future work.

The analysis that follows addresses the connection between discrete-time passivity and the conservation properties of collision response algorithms. §5.6.1 introduces some basic concepts of unilateral constraints, collision response, and energy conservation, while §5.6.2 discusses the conservation properties of various collision response algorithms. §5.6.3 shows that energy conservation in collision response, in conjunction with an energy conserving numerical integrator, leads to a discrete-time passive multibody simulation algorithm.

5.6.1 Basic concepts of unilateral constraints

A collision between two bodies is an extremely complicated event, often featuring fast time constants, deformations of the bodies, shock waves, vibrations, and energy lost to friction and plastic strain. In modeling such a system, the goal is to create the simplest model possible that captures all the "relevant" behavior. In many situations, if the bodies involved do not deform very much, a rigid-body assumption is used. This assumption greatly simplifies the dynamics of the system, and often produces useful results for the analyst.

It is important to remember, however, that perfectly rigid bodies do not exist. By basing the model on a fictional entity, the analyst is forced into postulating a set of dynamical rules that govern their behavior. For example, it is generally accepted that rigid bodies should be subject to Newton's laws of motion. These laws alone are sufficient to determine the motion of a rigid body system as long as there are no collisions between bodies. If collisions are allowed to occur, we must make additional assumptions governing these collisions. The following assumptions are often used in multibody simulations, and will be used in the present work:

- To prevent interpenetration of the bodies involved in the collision, body velocities must change instantaneously. Since finite forces cannot instantaneously change a body's velocity, the collision must generate an impulse. An impulse is an infinite force that lasts for an infinitesimal period of time, and whose time integral is non-zero.
- Because a collision takes an infinitesimal period of time to occur, the body configurations will be assumed constant throughout the collision.
- Due to the instantaneous nature of collisions, the effect of non-impulsive external forces on body velocities will be neglected during the course of the collision.

To obtain a full set of motion equations governing collisions, additional assumptions must be made. These additional equations are derived not from Newton's laws or other fundamental principles, but rather from empirical models used to approximate the complex behavior of collisions between bodies. Usually, these models try to predict how much energy is lost due to plastic deformation and friction during the collision. It is through the arbitrary nature of the contact model that problems can occur in haptic display.

As with numerical integration techniques, we must evaluate the "goodness" of collision response algorithms. There are three primary techniques used to evaluate a given set of approximations: comparison with a higher order approximation (e.g., a

Hertzian contact model), comparison with experimental measurements, and checking to see if the model can create kinetic energy. This latter technique carries the most relevance for haptic display, as there is a connection between the conservation and passivity properties of collision response algorithms.

5.6.2 Energy conserving collision response

Figure 5.7 shows a system of two rigid bodies β and γ the instant that they collide. Using the notation of (Smith 1991), we will express the collision equations of motion in terms of the relative velocity between the contact points, the impulse applied to each body as a result of the collision, and the contact inertia matrix. Since the contact inertia matrix depends only on the geometry of the collision ($\mathbf{x}(t)$, $\mathbf{y}(t)$, $\mathbf{r}_{bp}$, $\mathbf{r}_{cp}$, $\mathbf{b}$ and $\mathbf{c}$) and the inertial properties of the bodies involved, it will remain constant throughout the collision.

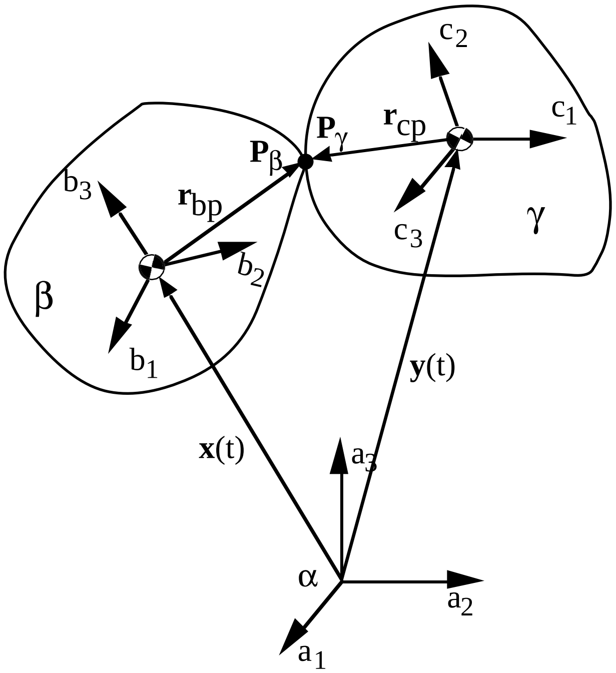

Figure 5.7. Two rigid bodies at the instant of collision. Vectors **x**(t) and **y**(t) describe the mass center locations of each of the two bodies in inertial frame α. $\mathbf{P}_\beta$ and $\mathbf{P}_\gamma$ are the contact points on each body, and $\mathbf{r}_{bp}$ and $\mathbf{r}_{cp}$ describe the location of $\mathbf{P}_\beta$ and $\mathbf{P}_\gamma$ with respect to the mass centers of β and γ respectively. Local coordinate systems (b_1,b_2,b_3) and (c_1,c_2,c_3) can be used to describe the orientation of bodies β and γ with respect to α.

The equations of motion for the system describe the relationship between the relative contact velocity before (**v**) and after the collision (**w**):

$$\mathbf{g} = \mathbf{M}(\mathbf{w} - \mathbf{v}) \tag{5.41}$$

where **g** is the impulse applied to body β (-**g** is applied to body γ), and **M** is the 3x3 contact inertia matrix. These equations express conservation of momentum for the entire system during the collision. It is important to note that three additional equations are necessary to compute the impulse itself, making a total of six equations to specify the change in velocities due to the collision. These additional equations are based on the assumptions made about the collision process.

To determine if a given algorithm is energy-conserving, we must evaluate the kinetic energy change as a result of the contact model. The change in kinetic energy for the system in Figure 5.1 can be expressed in several useful forms (Smith 1991):

$$\begin{aligned} \Delta K &= \frac{1}{2}\mathbf{w}^T\mathbf{M}\mathbf{w} - \frac{1}{2}\mathbf{v}^T\mathbf{M}\mathbf{v} \\ &= \frac{1}{2}\mathbf{g}^T(\mathbf{v}+\mathbf{w}) \\ &= \mathbf{g}^T\mathbf{v} + \frac{1}{2}\mathbf{g}^T\mathbf{M}^{-1}\mathbf{g} \end{aligned} \tag{5.42}$$

Energy growth due to poorly formed contact models has been observed by many researchers. The most cited example involves the interaction between Newton's model of restitution and Coulomb friction (Lotstedt 1984, Smith 1991, Wang and Mason 1992). Even in planar systems, the interaction between the two models results in energy growth for certain configurations. Routh's method (Routh 1905), by contrast, has been analytically demonstrated to conserve energy in all planar configurations (Wang and Mason 1992). Extension of the algorithm, which uses Poisson's hypothesis as a restitution model, to three dimensions is addressed in (Keller 1986, Mirtich and Canny 1994). Another method, proposed by Stronge(Stronge 1990), has also been demonstrated to conserve energy for rigid body collisions with Coulomb friction.

5.6.3 Discrete-time passive collision response

The importance of energy conservation for our application again relates to the incremental passivity condition covered in §5.2. Since the time step and configuration don't change during the course of a collision, (5.1) will be met if the stored energy decreases or remains constant as a result of the collision:

$$E'_k \leq E_k \tag{5.43}$$

where E'_k indicates the stored energy after the collision. As with the numerical integrators, a physically motivated choice for the storage function is the kinetic energy of the masses involved with the collision. Thus, any collision response algorithm that cannot generate energy will comply with the definition of discrete-time passivity. This result can serve as a guideline in choosing models of restitution and friction. In (Chang and Colgate 1997), Routh's method was used in a planar impulse-based simulation for haptic display, with good results from the point of view of passivity. However, the Newton/Coulomb contact model was not implemented for comparison, so it is possible the energy growth documented above is insignificant in practice.

This chapter has shown that if the numerical methods used in a physics-based simulation meet a specific incremental energy conservation guideline, they will be discrete-time passive. This result establishes, in the language of physics-based simulations, guidelines for these methods so that they can be used with a properly designed virtual coupling to create robust multibody simulations for haptic display. The next chapter explores the ramifications of these requirements in terms of their suitability in a real-time context.

CHAPTER 6

IMPLICIT VS. EXPLICIT FORMULATIONS

This chapter addresses some of the practical considerations of using these numerical methods in a "hard" real-time context.[*] In particular, §6.1 introduces the concept of explicit and implicit formulations in a real-time simulation, paying particular attention to integration methods. §6.2 demonstrates the relevance to the passivity theory of previous chapters by proving that discrete-time passive numerical operators require the solution of implicit equations. These results imply a natural tradeoff between robustness and ease of real-time implementation.

6.1 Delayed vs. non-delayed integrators - real time implementation

One important characteristic of a physics-based numerical method is whether it is delayed or non-delayed. A discrete numerical operator is *delayed* if its output does not depend on the most recent input, whereas it is *non-delayed* if the output does depend on the most recent input. Equivalently, a delayed operator is *strictly proper*, whereas a non-delayed operator is *proper but not strictly proper*. Since the virtual environment output immediately affects the input (via the virtual coupling), the formulation will be implicit

[*] For physics-based simulation, *hard* real-time means that the computational time is *guaranteed* to be smaller than simulation step size for all motions. Simulations used for animation, or even visual virtual reality, do not require this type of guarantee, as occasional delays do not typically have serious consequences.

unless the physics-based simulation has at least a one time step delay. This characteristic has important ramifications both for discrete-time passivity and for software implementation.

As a means of exploring how implicit and explicit formulations, let us return to the point mass example of Chapter 5. Figure 6.1 shows the discrete portion of a haptic display simulating an admittance causality 1 DOF point mass and using a delayed Euler integrator with a spring-damper virtual coupling.

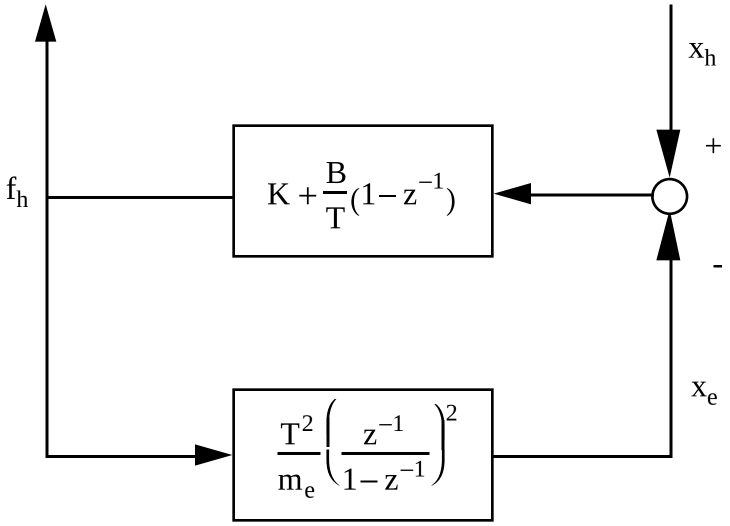
x_h
+
f_h
$K + \frac{B}{T}(1 - z^{-1})$
-
x_e
$\frac{T^2}{m_e}\left(\frac{z^{-1}}{1 - z^{-1}}\right)^2$

Figure 6.1. Delayed Euler mass simulation and virtual coupling block diagram. Parameters *K* and *B* are the virtual coupling stiffness and damping, *T* is the sample time, and m_e is the mass of the simulated environment.

The difference equations for this system are:

(6.1) $$f_{h,k} = \left(K + \frac{B}{T}\right)\left(x_{h,k} - x_{e,k}\right) - \frac{B}{T}\left(x_{h,k-1} - x_{e,k-1}\right)$$

(6.2) $$x_{e,k} = 2x_{e,k-1} - x_{e,k-2} + \frac{T^2}{m_e} f_{h,k-2}$$

By looking at (6.2) we can see that $x_{e,k}$ does not depend on $f_{h,k}$, but rather on $f_{h,k-2}$. This dependence means that the calculation at each time can be broken into two steps. The first step is to calculate $x_{e,k}$, which depends only on old values of the virtual coupling force. The second is to calculate $f_{h,k}$ based on the most recent position value from the sensors and virtual environment simulation. This force is immediately sent back to the haptic display hardware, but will not affect the environment output until two more position measurements, $x_{h,k}$ and $x_{h,k-1}$, arrive from the sensors.

Figure 6.2 again shows the discrete portion of a haptic display simulating a 1 DOF point mass. This time, however, it is using a non-delayed Euler integrator with the spring-damper virtual coupling. The difference equation for the virtual coupling remains the same, but the one for the environment becomes:

(6.3) $$x_{e,k} = 2x_{e,k-1} - x_{e,k-2} + \frac{T^2}{m_e} f_{h,k}$$

The primary difference is that $x_{e,k}$ now depends directly on $f_{h,k}$, making it impossible to split the calculation into two distinct steps. There are two approaches to calculating $f_{h,k}$: *combination* and *iteration*. In "combination", the pulse transfer function from f_h to x_h is

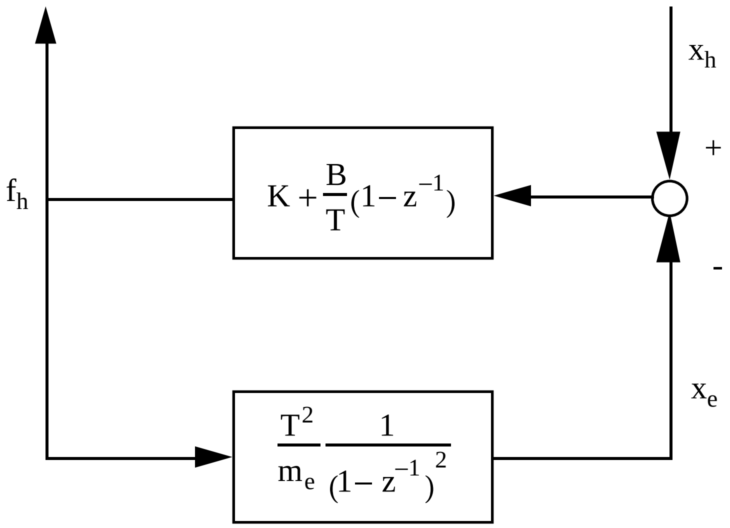

x_h
+
-
x_e
f_h
$K+\frac{B}{T}(1-z^{-1})$
$\frac{T^2}{m_e}\frac{1}{(1-z^{-1})^2}$

Figure 6.2. Non-delayed Euler mass simulation and virtual coupling. Parameters *K* and *B* are the virtual coupling stiffness and damping, *T* is the sample time, and *m_e* is the mass of the simulated environment.

calculated directly through block diagram manipulation, and then converted into difference equations:

(6.4)
$$\frac{f_h(z)}{x_h(z)}=\frac{\left[KT^2+BT\left(1-z^{-1}\right)\right]\left(1-z^{-1}\right)^2}{\frac{KT^2}{m_e}+\frac{BT}{m_e}\left(1-z^{-1}\right)+\left(1-z^{-1}\right)^2}$$

(6.5)
$$f_k=\frac{\left(2+\frac{BT}{m_e}\right)f_{k-1}-f_{k-2}+\left(K+\frac{B}{T}\right)h_k-\left(2K+\frac{3B}{T}\right)h_{k-1}+\left(K+\frac{3B}{T}\right)h_{k-2}-\frac{B}{T}h_{k-3}}{1+\frac{KT^2}{m_e}+\frac{BT}{m_e}}$$

where the subscript on f_h has been dropped and x_h has been replaced by h for compactness. The extension to more complicated environments, where integration, collision detection, and collision response would all be combined into one nonlinear formulation, makes this approach unworkable. Iteration is the normal technique used to solve implicit equations, but would require extremely careful consideration of efficiency and convergence, due to the unilateral constraints present in multibody simulations.

6.2 Delayed vs. non-delayed integrators - discrete time passivity

From the previous section it is clear that delayed methods are significantly easier to use in hard real time simulations and offer substantial computational savings compared to their non-delayed counterparts. In this section, we address the issue of discrete-time passivity of these operators. Continuing with the example of the previous section, we can evaluate the discrete-time passivity of a simulation operator by looking at the mapping from virtual coupling force to environment position change. For the delayed and non-delayed Euler method, respectively, this transfer function is:

(6.6) Delayed Euler: $$\frac{\Delta x_e(z)}{f_h(z)} = \frac{T^2}{m_e}\frac{z^{-2}}{1-z^{-1}}$$

(6.7) Non-delayed Euler: $$\frac{\Delta x_e(z)}{f_h(z)} = \frac{T^2}{m_e}\frac{1}{1-z^{-1}}$$

Since both operators are linear, their discrete-time passivity can be assessed by looking at the real part of each transfer function evaluated along the Nyquist Contour:

(6.8) Delayed Euler:
$$\mathrm{Re}\left\{\frac{\Delta x_e(z)}{f_h(z)}\right\}_{z=e^{j\omega T}} = -\frac{T^2}{m_e}\frac{1+2\cos\omega T}{2}$$

(6.9) Non-delayed Euler:
$$\mathrm{Re}\left\{\frac{\Delta x_e(z)}{f_h(z)}\right\}_{z=e^{j\omega T}} = \frac{1}{2}$$

From (6.8), we can see that the delayed Euler method is not discrete-time passive because the real part of the transfer function from force to position change can be negative. The non-delayed Euler method, on the other hand, is shown to be discrete-time passive in (6.9) because the real part of the transfer function is guaranteed to be positive. Within this simple linear example, there is a clear tradeoff between efficiency and robustness. The ideal numerical integrator, of course, would be one that is delayed and discrete-time passive, and this example serves as motivation for the search.

To determine whether there exists delayed discrete time passive numerical methods, we must generalize the notation somewhat to allow for nonlinear operators. Consider an arbitrary discrete operator *G* acting on input *u* and resulting in output *y*:

(6.10)
$$y_k = G(u_k, y_{k-1}, u_{k-1}, y_{k-2}, u_{k-2}, \ldots, y_1, u_1, y_0, u_0)$$

where u_k and y_k are assumed to be zero for negative values of *k*. If *G* is delayed, then the dependence on u_k is removed:

(6.11) $$y_k = G\left(y_{k-1}, u_{k-1}, y_{k-2}, u_{k-2}, \ldots, y_1, u_1, y_0, u_0\right)$$

From basic passivity definitions given in Chapter 2, *G* is discrete-time passive iff:

(6.12) $$\sum_{k=0}^{N} u_k \cdot y_k \geq -E_0 \qquad \forall\ N \in \mathbb{Z}^+$$

which can be rewritten as:

(6.13) $$u_N y_N \geq -E_0 - \sum_{k=0}^{N-1} u_k \cdot y_k \qquad \forall\ N \in \mathbb{Z}^+$$

Since y_N depends only on previous values of *u* and *y*, u_N can be selected such that this expression will be violated:

(6.14) $$\begin{aligned} y_N > 0:\ \ u_N &< -\frac{E_0 + \sum_{k=0}^{N-1} u_k y_k}{y_N} \\ y_N < 0:\ \ u_N &> -\frac{E_0 + \sum_{k=0}^{N-1} u_k y_k}{y_N} \end{aligned}$$

The only case where u_N cannot be selected to violate (6.12) is when $y_N=0$ for all *N*. Since any non-trivial explicit method must be discrete-time active, it follows that all discrete*N*-time passive numerical operators must be delayed.

This result somewhat weakens the analyses of the previous two chapters, because it says that the goal of discrete-time passivity for real-time simulations is unreachable for all but very simple virtual environments. Without the guarantee of discrete-time passivity, the *complete* separation between environment dynamics and device passivity is also unreachable. However, our experience to date has shown that, while not discrete-time passive, delayed numerical methods typically experience only a weak connection between environment dynamics and device passivity. For hand tool simulations, this connection takes the form of a minimum mass and inertia moment for the virtual tool. In the next chapter, we explore this issue in greater detail, developing passivity conditions and parameter limitations for simulations using explicit formulations.

CHAPTER 7

MINIMUM MASS FOR HAPTIC DISPLAY SIMULATIONS

This chapter investigates the connection between environment dynamics and device passivity for explicit formulations of admittance causality virtual environments. As an exploration into this topic, Section 7.1 considers the simulation of a 1-DOF point mass, with the virtual coupling structure outlined previously. In addition to being a good way of exploring the passivity characteristics for more general systems, the simulation of a mass is one of the critical building blocks for multibody simulations. This analysis uses one particular virtual coupling and several different numerical integrators. The passivity of these numerical methods is compared to that of a backwards-difference spring-damper virtual wall. Since all the virtual coupling and environment operators are linear, the derivations are straight forward using standard linear passivity tools. Section 7.2 introduces an improved tuning procedure for haptic displays with explicit formulations and presents some experimental results. Section 7.3 briefly discusses the application of these concepts to multibody virtual environments.

7.1 Haptic display passivity with delayed numerical integrators

Recall from Chapter 3 the analysis developed in (Colgate and Schenkel 1997), which formulated passivity conditions for systems with the structure shown in Figure 7.1. The most general result was an expression for the minimum physical damping necessary

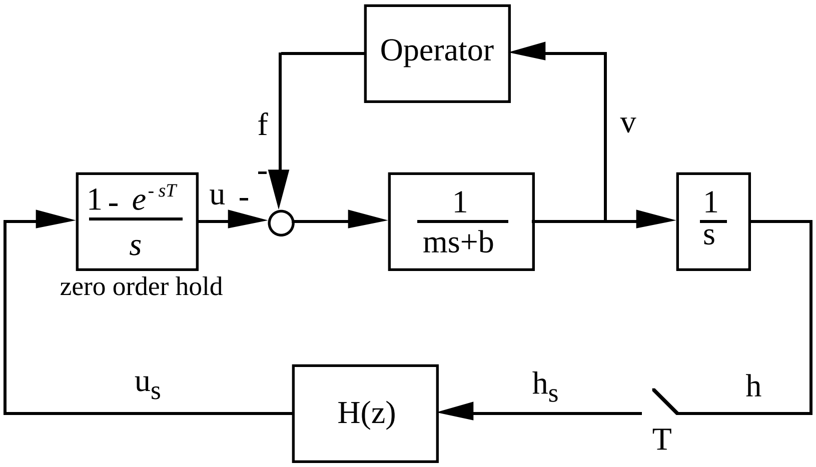

Figure 7.1. Colgate and Schenkel's model of a 1 DOF haptic display. The inherent inertia and damping of the haptic display handle are *m* and *b*, respectively. *H(z)* is the virtual environment, *T* is the sample time, *h* is the handle position and *u* is the actuator effort (*h_S* and *u_S* after sampling).

to ensure that the device would appear passive to the human operator, assuming linear virtual environment dynamics:

(7.1) $$b > \frac{T}{2}\frac{1}{1-\cos\omega T}\mathrm{Re}\left\{\left(1-z^{-1}\right)H(z)\right\}_{z=e^{j\omega T}} \qquad 0 \le \omega \le \omega_S$$

For the present analysis, we use linear virtual coupling (*C(z)*) and environment (*E(z)*) models, resulting in the following transfer function for their combined dynamics:

(7.2) $$H(z) = \frac{C(z)}{1 + C(z)E(z)}$$

The virtual coupling used throughout this analysis, a backwards difference damped spring, was chosen based on its simplicity and because other couplings have not been shown to perform better in practice.

$$C(z) = K + \frac{B}{T}\left(1 - z^{-1}\right) \tag{7.3}$$

We will consider three different delayed numerical integrators (see Table 1).

Numerical Method	Difference Equations	Transfer Function
Method 1 Delayed Euler velocity Delayed Euler position	$v_k = v_{k-1} + \frac{T}{m_e} f_{k-1}$ $x_k = x_{k-1} + T v_{k-1}$	$\frac{x(z)}{f(z)} = \frac{T^2}{m_e} \frac{z^{-2}}{\left(1 - z^{-1}\right)^2}$
Method 3 Delayed Euler velocity Non-delayed Euler position	$v_k = v_{k-1} + \frac{T}{m_e} f_{k-1}$ $x_k = x_{k-1} + T v_k$	$\frac{x(z)}{f(z)} = \frac{T^2}{m_e} \frac{1}{\left(1 - z^{-1}\right)^2}$
Method 3 Delayed Euler velocity Trapezoidal position	$v_k = v_{k-1} + \frac{T}{m_e} f_{k-1}$ $x_k = x_{k-1} + T \frac{v_{k-1} + v_k}{2}$	$\frac{x(z)}{f(z)} = \frac{T^2}{2m_e} \frac{\left(1 + z^{-1}\right) z^{-1}}{\left(1 - z^{-1}\right)^2}$

Table 1. Transfer functions and difference equations for three delayed numerical integrators

Substitution of the expressions for the virtual coupling and environment dynamics into (7.1) and (7.2) results in three different passivity conditions. Method 1 uses the delayed Euler method to update position, resulting in the following combined environment and virtual coupling dynamics:

$$(7.4) \qquad H_1(z) = \frac{K + \frac{B}{T}\left(1 - z^{-1}\right)}{1 + \frac{T^2}{m_e}\frac{z^{-2}}{\left(1 - z^{-1}\right)^2}\left[K + \frac{B}{T}\left(1 - z^{-1}\right)\right]}$$

Substitution into (7.1) yields the passivity conditions for the haptic display:

$$(7.5) \qquad b_1 > \frac{T}{2}\frac{1}{1 - \cos\omega T}\operatorname{Re}\left\{\frac{\left(1 - z^{-1}\right)^3\left[K + \frac{B}{T}\left(1 - z^{-1}\right)\right]}{\left(1 - z^{-1}\right)^2 + \frac{T^2}{m_e}\left[K + \frac{B}{T}\left(1 - z^{-1}\right)\right]z^{-2}}\right\}_{z=e^{j\omega T}}$$

The difficulty here is that the required damping is a function of four independent system parameters: *K*, *B*, *T*, and *m*. Converting this condition to non-dimensional form can reduce the number of parameters, making it easier to identify trends within the data. For the analysis that follows, we reduce the total number of parameters from five to three by introducing the following dimensionless quantities:

$$(7.6) \qquad b^* = \frac{b}{b_{wall}} \qquad \alpha = \frac{KT^2}{m_e} \qquad \beta = \frac{B}{KT}$$

The first dimensionless parameter, b^*, normalizes the required physical damping for the mass simulation by the physical damping required for a backwards difference virtual wall. If b^* is greater than unity for a given set of dimensioned parameters, more physical damping will be required than for a virtual wall of the same stiffness and damping. The second non-dimensional parameter, α, represents the natural frequency associated with the virtual coupling's spring and the virtual environment's mass, scaled against the update rate of the controller. The final dimensionless parameter, β, represents the amount of virtual coupling damping relative to the stiffness.*

Before continuing with the analysis, recall the passivity condition for a backwards difference damped-spring virtual wall:

$$b > \frac{KT}{2} + B \tag{7.7}$$

To simplify comparisons with other simulations, it is useful to include the dimensionless parameter β, resulting in the following expression for the minimum physical damping to ensure passivity for a virtual wall:

$$b_{\text{wall}} = \frac{KT}{2}(1 + 2\beta) \tag{7.8}$$

It is this expression that is used to non-dimensionalize the physical damping of the device in (7.6). Using the dimensionless parameters, the passivity condition for Method 1 becomes:

$$b_1^*(\omega T) \geq \frac{1}{1+2\beta} \cdot \frac{1}{1-\cos\omega T} \cdot \operatorname{Re}\left\{ \frac{\left(1+\beta-\beta z^{-1}\right)\left(1-z^{-1}\right)^3}{\left(1-z^{-1}\right)^2 + \alpha\left(1+\beta-\beta z^{-1}\right)z^{-2}} \right\}_{z=e^{j\omega T}} \tag{7.9}$$

* An alternative to this choice is $\beta = B/\sqrt{Km}$. This selection ends up being inconvenient because it contains the virtual environment mass, making comparisons with virtual walls more difficult.

While still not a tractable analytic solution, (7.9) can at least be explored graphically. Figure 7.2 uses level curves of b^* to show the region in α-β space where the passivity condition for each simulation matches that of the virtual wall (i.e., $b^*=1$). In regions where the ratio is less than or equal to unity, (7.7) is sufficient to determine passivity of the device. In essence, b^* is a measure of activeness, relative to the activeness of the virtual wall.

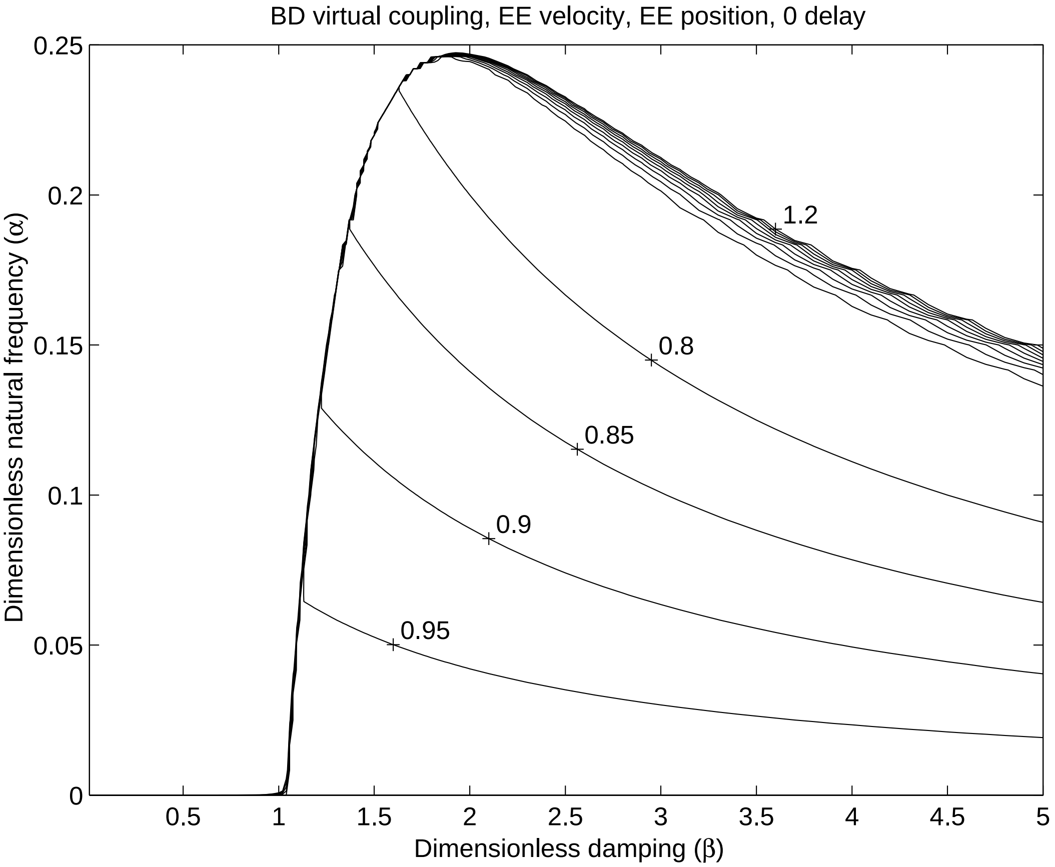

Figure 7.2. Level curves of required damping (b*) for a virtual mass using the delayed Euler method to update position and velocity. For values less than or equal to one, the system will be passive if (7.7) is also met. Level curves above *b*=1.2* are not shown.

To interpret this graph, it is useful to step through the environment design process in terms of the dimensioned parameters, *K*, *B*, *m*, and *T*. Selection of the stiffness, damping and update rate determines β, and thus the position on the abscissa, along with the scale factor of *1/m* on the ordinate. Regardless of this selection, decreasing *m* will eventually lead to crossing the unity level curve (i.e., the required physical damping will exceed that necessary for a comparable virtual wall). For example, typical values of *K*, *B*, and *T* for the 1-DOF device in our lab are:

(7.10) $$K=10^4 \text{ (N/m)} \qquad B=20 \text{ (N·sec/m)} \qquad T=0.001 \text{ (sec)}$$

resulting in the dimensionless parameters:

(7.11) $$\beta=2 \qquad \alpha=\frac{0.00025}{m}$$

where *m* is the virtual environment mass expressed in kilograms. Equation (7.11) describes a vertical line in the α-β plane. This line crosses the $b^*=1$ level curve at $\alpha\approx0.24$. Solving for *m* at this intersection yields the mass at which the required physical damping exactly equals the damping required for the virtual wall:

(7.12) $$m\approx0.04 \text{ (kg)}$$

Simulation of masses smaller than this value will require more physical damping than a backwards difference spring damper virtual wall with parameters given by (7.10).

Figure 7.3 shows more generally how the dimensionless parameters α and β are affected by each of the dimensioned parameters.

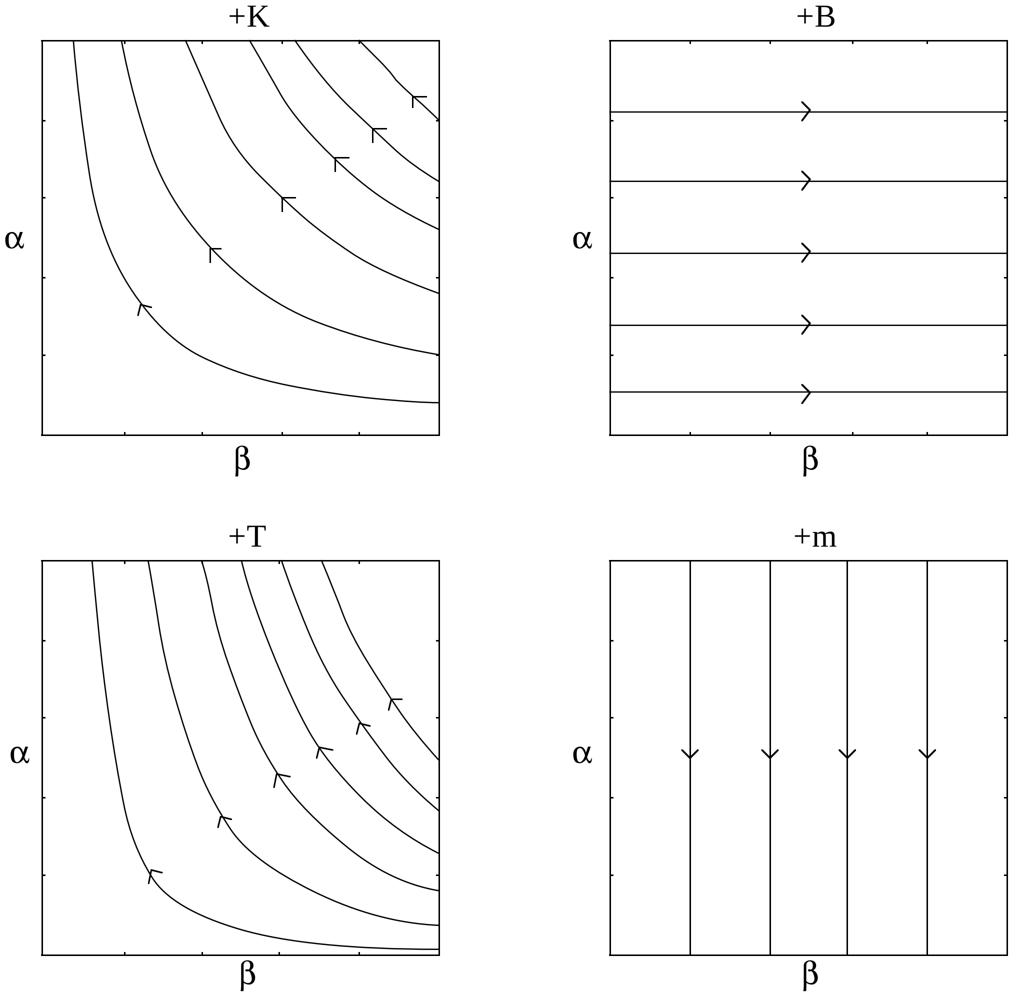

Figure 7.3. Graphical demonstration of how the dimensionless parameters α and β are affected by the dimensioned parameters *K*, *B*, *T*, and *m*. The arrows indicate the direction of increase for each dimensioned parameter.

A parallel analysis yields similar passivity conditions for the two additional numerical integrators. Method 2 uses the non-delayed Euler method to update position, while

Method 3 uses the trapezoidal rule for position updates. Substitution of the appropriate transfer functions from Table 1 into (7.1) and conversion to dimensionless parameters results in passivity conditions for these two implementations:

$$(7.13) \qquad b_2^*(\omega T) \geq \frac{1}{1+2\beta} \cdot \frac{1}{1-\cos\omega T} \cdot \mathrm{Re}\left\{ \frac{\left(1+\beta-\beta z^{-1}\right)\left(1-z^{-1}\right)^3}{\left(1-z^{-1}\right)^2 + \alpha\left(1+\beta-\beta z^{-1}\right)z^{-1}} \right\}_{z=e^{j\omega T}}$$

$$(7.14) \quad b_3^*(\omega T) \geq \frac{1}{1+2\beta} \cdot \frac{1}{1-\cos\omega T} \cdot \mathrm{Re}\left\{ \frac{\left(1+\beta-\beta z^{-1}\right)\left(1-z^{-1}\right)^3}{\left(1-z^{-1}\right)^2 + \frac{1}{2}\alpha\left(1+\beta-\beta z^{-1}\right)\left(1+z^{-1}\right)z^{-1}} \right\}_{z=e^{j\omega T}}$$

As with Method 1, tractable analytic solutions are evasive, but graphical methods are sufficient due to the reduced number of independent parameters. Figures 7.4 and 7.5 again use level curves of b^* to show the region in α-β space where the passivity condition for each simulation matches that of the virtual wall. Notable features of these graphs include:

- For delayed Euler position updates (Method 1, Figure 7.2), β must be greater than one to achieve passivity. Below the unity level curve, b^* is weakly dependent on α and β.
- For non-delayed Euler position updates (Method 2, Figure 7.4), more damping is required for mass simulations than for virtual walls. However, the gradient of the required damping is fairly low, so that if the virtual wall is allowed to be somewhat softer than optimal, a reasonable range of masses can be simulated passively.

- For trapezoidal position updates (Method 3, Figure 7.5), β must be greater than *1/2* to achieve passivity. The region under the unity level curve is perfectly flat, indicating that the values of α and β will not affect passivity at all within this region. Of the three methods considered, Method 3 allows the smallest masses to be simulated, both in theory and in practice.

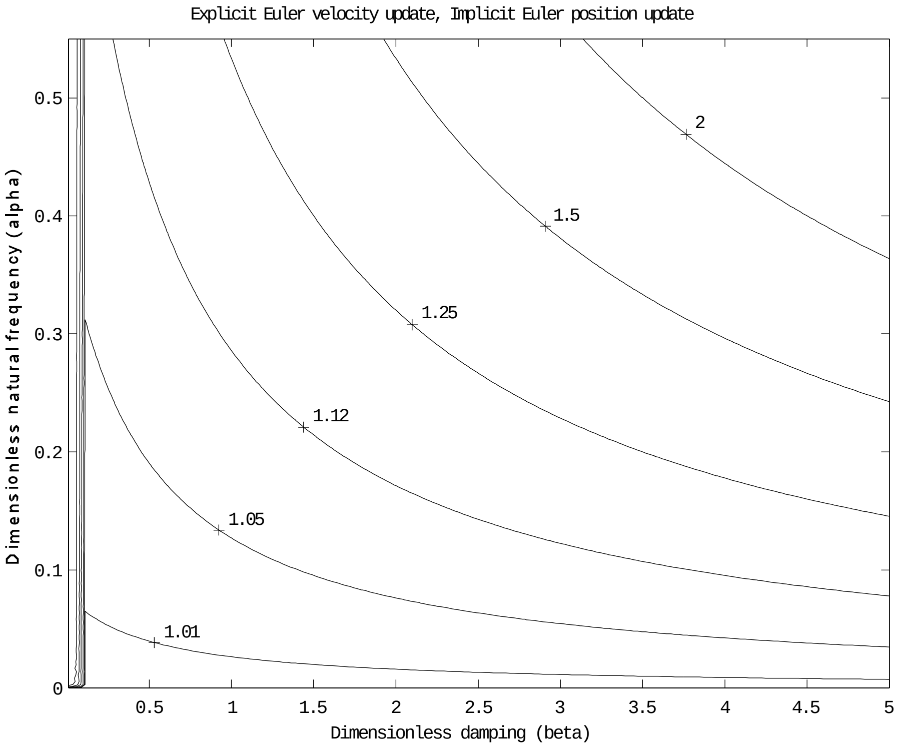

Figure 7.4. Level curves of required damping for a virtual mass using non-delayed Euler position updates. Note that with this integrator, more damping is always required for mass simulations than for wall simulations. If stiffness and damping are less than that required by (7.7), then mass simulations can be passive.

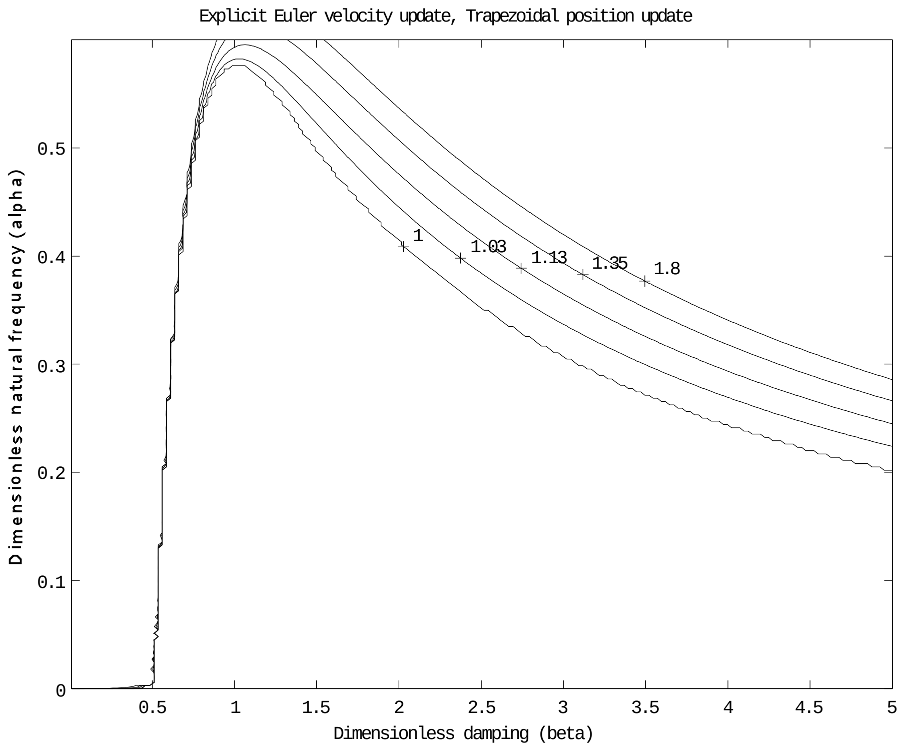

Figure 7.5. Level curves of required damping for a virtual mass using trapezoidal position updates. For this integrator, there is a wide region under the unity level curve where the required damping exactly matches that of the virtual wall. As long as α and β fall within this region, their values do not affect passivity.

To get a sense for how these restrictions in α-β space affect the dimensioned parameters, one can fit an analytic function to the unity level curve. For Method 3, a reasonable approximation is given by (7.15), and is shown graphically in Figure 7.6:

$$\alpha < \frac{\beta}{\beta^2 + 0.732\beta + 0.25}, \ \beta > \frac{1}{2} \tag{7.15}$$

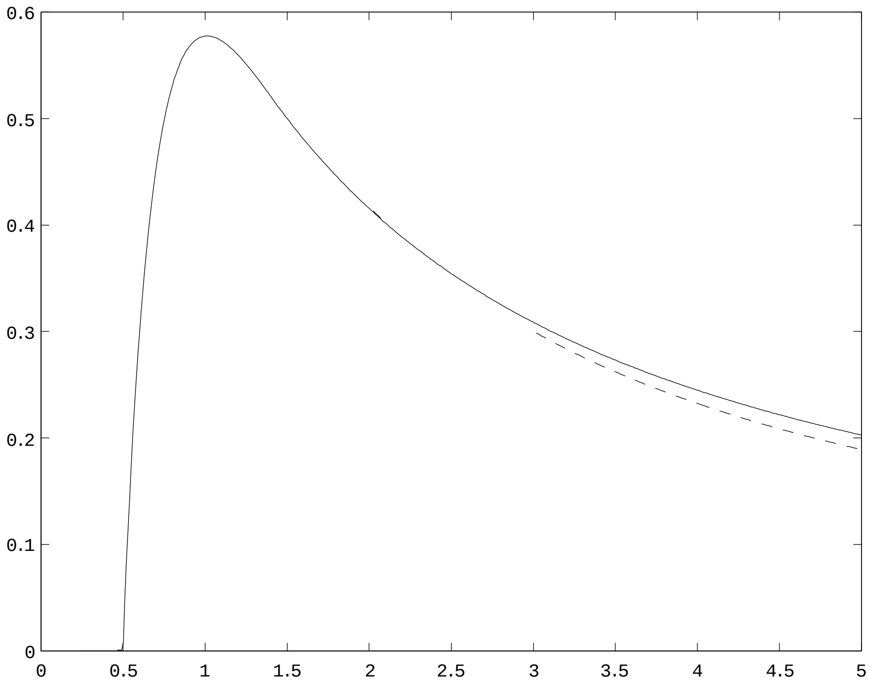
0.6
0.5
0.4
0.3
0.2
0.1
0
0
0.5
1
1.5
2
2.5
3
3.5
4
4.5
5

The first condition is simply the normal virtual wall result, the second places a limitation on the virtual coupling damping, and the final indicates a minimum mass that can be simulated safely.

The importance of these results is not the exact value of the minimum mass or the quality of the analytic approximation, but rather that the minimum mass exists in the first place. As long as the mass is kept above this value, passivity is guaranteed. This result corroborates our experiences when implementing multibody simulations with a virtual coupling -- if the mass (or moment of inertia) drops too low, the user can elicit oscillations from the haptic display handle. If the mass is kept above this minimum, the simulations are exceptionally reliable.

7.2 An improved tuning procedure

Due to the complexity of the passivity analysis, identification of the minimum mass is best handled experimentally. One procedure that works well in practice is to go through the following four steps:

1) Select the update rate based on the complexity of the physics-based simulation and the computational resources available. For multibody simulations involving collisions between rigid bodies, an update rate of 500 Hz or higher allows collisions to feel reasonably rigid. As a rule of thumb, update rates below 100-200 Hz tend to suffer from poor perceptual quality and/or stability problems.

2) Given the update rate, identify the maximum virtual stiffness and damping through simulation of virtual walls and bodies of infinite mass (i.e., bilateral virtual walls).

3) Given the update rate, stiffness and damping, identify the minimum mass and moment of inertia associated with the numerical method of choice. To date, the best integration method we have identified uses first and second order Taylor's approximations for velocity and position update, respectively.

4) If lower masses are required, then a tradeoff can be made by dropping the virtual coupling stiffness and damping. As the stiffness (and damping) approaches the maximum identified in Step 2, this tradeoff can be quite beneficial, because small changes in virtual coupling stiffness lead to relatively large changes in minimum mass in this region.

This parameter tuning procedure is more effective than previous techniques. It is fundamentally motivated by the passivity results obtained in the previous section and results in extremely robust behavior. To indicate how this process works in practice, a simple experiment was performed on the 1 DOF haptic display in our lab (Figure 7.7).

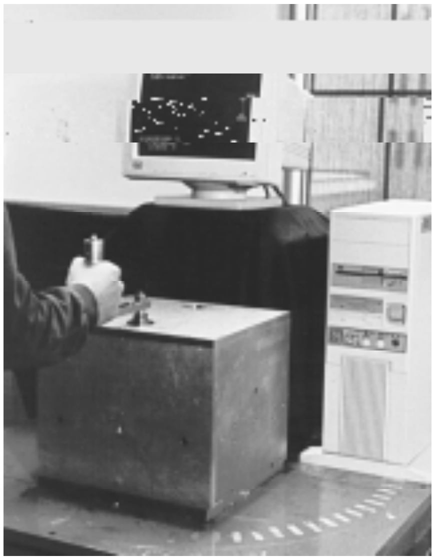

Figure 7.7. One DOF haptic display used to obtain experimental results.

The device is powered by a DC brushless motor mounted to a sturdy table so that the motor shaft points upward. Attached to the shaft is a crank handle that the user may grab with his/her hand. An optical encoder on the motor shaft measures position with a resolution of 900,000 counts per revolution (this extremely fine position resolution allows numerical differentiation to be reasonably accurate even at high update rates). Motor currents are supplied by a pulse width modulating amplifier, and voltage inputs to the amplifier are provided by a 12-bit A/D converter. Because the device is equipped with a fluid-filled viscous damper, it can simulate a wide range of impedances passively. See (Chang 1994) and (Brown 1995) for details on the hardware configuration.

For Step 1, the update rate was chosen somewhat arbitrarily to be 1000 Hz. The computational time for a simple mass integrator was approximately 0.1 ms, making the effect of computational delay relatively small. For Step 2, the dimensionless damping ratio β was set to one in order to maximize the allowable range of natural frequencies (see Figure 7.5). The maximum stiffness for a bilateral backwards difference damped spring was measured to be approximately 12,400 (N/m) at the handle. For Steps 3 and 4, the minimum mass was measured over a range of virtual coupling stiffness. Figure 7.8 shows the results of these steps, along with the theoretical predictions based on the passivity analysis.[*]

The experimental results capture the essential nature of the passivity analysis. They indicate that the minimum mass becomes infinite as the virtual coupling stiffness approaches the maximum possible for the device, and show how smaller masses can be simulated passively through a tradeoff with virtual coupling stiffness. Possible sources of error in the theoretical analysis include oversimplified mechanism dynamics (this

[*] The device damping used in the model was measured indirectly in Step 2 by assuming that $b>KT/2+B$ to preserve passivity.

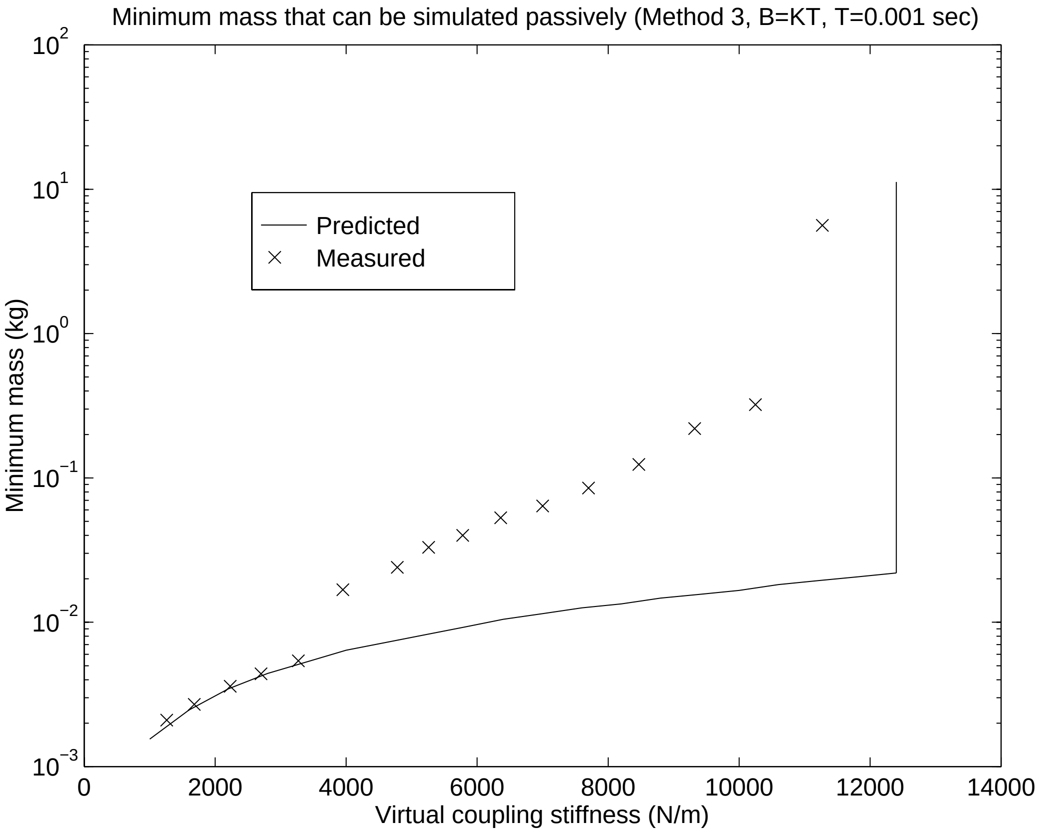

Figure 7.8. Minimum mass as a function of virtual coupling stiffness for the 1 DOF haptic display. The vertical line is an asymptote at which the minimum mass becomes infinite.

analysis used a damped mass), unmodeled computational delay, and operator inability to destabilize slightly active systems. The first two potential sources of error are currently being addressed through extension of the mechanism and environment model. Incorporation of computational delay will increase the predicted minimum mass, while an improved mechanism model could result in increased or decreased minimum mass. Human operator limitations are an inherent difficulty with experimental verification of passivity, and would tend to decrease the measured minimum.

7.3 Extension to multibody simulations

This type of tuning procedure has proven to be extremely reliable on two higher degree of freedom haptic displays in our lab (Figure 7.9).

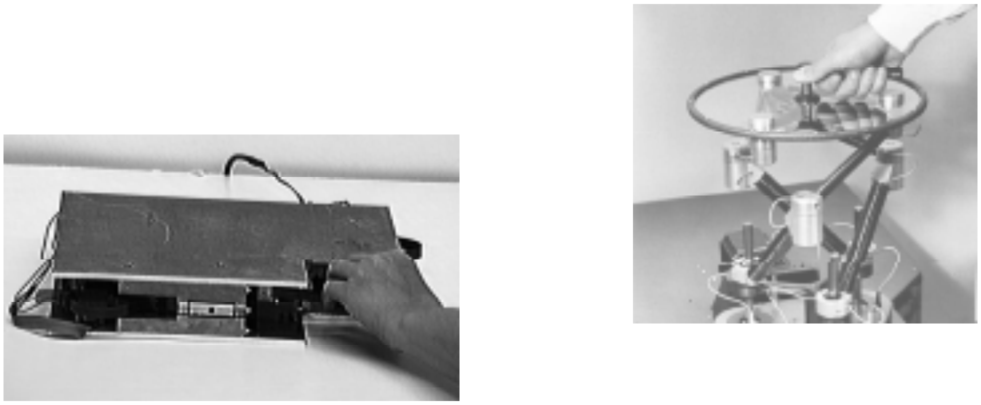

1997). Anecdotal experiences are quite promising, as the simulator exhibits vastly improved stability properties compared to previous implementations. Details of the implementation can be found in and (Chang 1998).

CHAPTER 8

CONCLUSIONS AND FUTURE WORK

This thesis has addressed the development of complex virtual environment simulations for haptic interfaces. On a practical level, the contribution of the work is that we have developed a hardware/software architecture that permits the simulation of complex multibody environments on a haptic display. These simulations exhibit vastly improved stability properties compared to previous implementations.

The theoretical developments of Chapter 4 represent a significant generalization of previous passivity theory conducted in our research group. Previously, the only virtual coupling passivity analysis that existed was based on numerical techniques (structured singular values). While the specific passivity analyses presented in Chapter 4 are original, the virtual coupling used with impedance causality virtual environments was directly inspired by Adams and Hannaford (Adams, et al. 1998). One possible future avenue of research is extension of the theory to multiple degrees of freedom. While mathematically difficult, this extension appears to present no conceptual problems. It is not clear, however, that it would produce any new insight into hardware or software design. Other, more promising lines include incorporation of higher order mechanism models into the analysis and optimization of the virtual coupling. While the spring-damper version has clear physical motivation and works quite well in practice, other options may work more effectively (e.g., transmission lines).

Establishing the connection between the incremental conservation properties of physics-based numerical methods and the discrete-time passivity of the mathematical operators is an original development. This connection is important because it forms a bridge between the vast literature of physics-based simulation and sampled-data control/stability issues that arise in haptics. It provides a simulation designer important guidance in selecting numerical methods for use with haptic virtual environments. The most obvious future work here is the development of discrete-time passive numerical integrators for three-dimensional rotations. Since these integrators would have to be implicit, it is not clear that this work would produce any directly usable results.

The proof that discrete-time passive operators must be implicit, while not a particularly challenging derivation, yields some important results. It shows that the exemplar of discrete-time passive physics-based simulations cannot be realized in "hard" real time for anything but very simple virtual environments. Future work includes the continued development of explicit numerical methods for use in haptic display simulations. Chapter 5 implies that the closer an integrator is to energy-conserving (and thus, to being discrete-time passive), the better it will perform when used with a virtual coupling in haptic simulations. Finding the proper metric for "closeness to energy conservation" would provide a useful way of contrasting different integrators.

The detailed passivity analysis in Chapter 7, while a straight forward application of previously derived passivity theory, shows that admittance causality mass simulations have a minimum mass that can be implemented passively. This development permits a useful restriction on the class of environments that can be simulated when using explicit numerical methods. Future work along these lines might explore the implementation of impedance causality environments with explicit numerical methods. As with admittance causality environments, the use of explicit numerical methods will force restrictions on the range of virtual environments that can be simulated passively. The form these restrictions will take has not yet been identified, but one hypothesis is that, analogous to the minimum mass for admittance environments, there exists a maximum stiffness for impedance environments.

REFERENCES

Adams, R. and Hannaford, B., 1998, "A Two-Port Framework for the Design of Unconditionally Stable Haptic Interfaces," *Proc. IEEE/RSJ International Conference on Intelligent Robots and Systems*, Victoria, B.C., Canada, ASME, accepted for publication.

Adams, R., Moreyra, M. R. and Hannaford, B., 1998, "Stability & performance of haptic displays: Theory and experiments," *Proc. International Mechanical Engineering Congress and Exhibition*, Anaheim, CA, ASME, accepted for publication.

Basdogan, C., Ho, C., Srinivasan, M. A., Small, S. D. and Dawson, S. L., 1998, "Force Interactions in Laparoscopic Simulations: Haptic Rendering of Soft Tissues," *Proc. Medicine Meets Virtual Reality*, San Diego, CA, IOS Press.

Baumann, R., Maeder, W., Glauser, D. and Clavel, R., 1996, "The pantoscope: a spherical remote-center-of-motion parallel manipulator for force reflection," *Proc. International Conference on Robotics and Automation*, Albuquerque, NM, IEEE, pp. 718-726.

Bostrom, M., Singh, S. K. and Wiley, C. W., 1993, "Design of An Interactive Lumbar Puncture Simulator With Tactile Feedback," *Proc. Virtual Reality Annual International Symposium (VRAIS)*, IEEE, pp. 280-286.

Brooks, F. P., Ouh-Young, M., Batter, J. J. and Kilpatrick, P. J., 1990, "Haptic Displays for Scientific Visualization," *Computer Graphics*, Vol. 24, No. 4, pp. 177-185.

Brown, J. M., 1995, "A Theoretical and Experimental Investigation Into the Factors Affecting the Z-Width of a Haptic Display," , M.S., Northwestern University.

Buttolo, P., Oboe, R., Hannaford, B. and McNeely, W., 1996, "Force Feedback in Shared Virtual Simulations," *Proc. International Conference on the CADCAM, Computer Graphics and Computer Aided Technologies (MICAD)*, Paris, France, Editions HERMES.

Chang, B., 1994, "On damped manipulator with damping compensation for the haptic interface in a virtual environment," , M.S., Northwestern University.

Chang, B., 1998, "Real-time impulse-based rigid body systems for haptic display," Ph.D., expected 10/98, Northwestern University.

Chang, B. and Colgate, J. E., 1997, "Real-time Impulse-based Simulation of Rigid Body Systems for Haptic Display," *Proc. International Mechanical Engineering Congress and Exhibition*, Dallas, TX, ASME, pp. 145-152.

Colgate, J. E., 1994, "Coordinate Transformations and Logical Operations for Minimizing Conservativeness in Coupled Stability Criteria," *Journal of Dynamic Systems, Measurement and Control*, Vol. 116, No. 4, pp. 639-649.

Colgate, J. E. and Brown, J. M., 1994, "Factors Affecting the Z-width of a Haptic Display," *Proc. International Conference on Robotics and Automation*, San Diego, CA, IEEE R&A Society, **4**, pp. 3205-10.

Colgate, J. E., Grafing, P. E., Stanley, M. C. and Schenkel, G., 1993, "Implementation of Stiff Virtual Walls in Force-Reflecting Interfaces," *Proc. Virtual Reality Annual International Symposium*, Seattle, WA, IEEE, pp. 202-207.

Colgate, J. E. and Schenkel, G. G., 1997, "Passivity of a Class of Sampled-Data Systems: Application to Haptic Interfaces," *Journal of Robotic Systems,* Vol. 14, No. 1, pp. 37-47.

Colgate, J. E., Stanley, M. C. and Brown, J. M., 1995, "Issues in the Haptic Display of Tool Use," *Proc. IEEE/RSJ International Conference on Intelligent Robots and Systems*, Pittsburgh, **3**, pp. 140-145.

Cotin, S., Delingette, H., Clement, J.-M., Tassetti, V., Marescaux, J. and Ayache, N., 1996, "Geometric and Physical Representations for a Simulator of Hepatic Surgery," *Proc. Medicine Meets Virtual Reality IV,* IOS Press, pp. 139-151.

Desoer, C. A. and Vidyasagar, M., 1975, Feedback Systems: Input-Output Properties, Academic Press, New York.

Durlach, N. and Mavor, A., 1994, "Virtual reality: scientific and technological challenges," Chapter 4 (Haptic Interfaces by M. Srinivasan).

Gibson, S., Samosky, J., Mor, A., Fyock, C., Grimson, E., Kanade, T., Kikinis, R., Lauer, H., McKenzie, N., Nakajima, S., Ohkami, H., Osborne, R. and Sawada, A., 1996, "Simulating Arthroscopic Knee Surgery using Volumetric Object Representations, Real-Time Volume Rendering and Haptic Feedback," Mitsubishi Electric Research Lab, Cambridge, MA, TR96-19.

Gillespie, R. B., 1996, "Haptic Display of Systems with Changing Kinematic Constraints: The Virtual Piano Action," , Ph. D., Stanford University.

Gillespie, R. B., 1997, "A Survey of Multibody Dynamics for Virtual Environments," *Proc. International Mechanical Engineering Conference and Exhibition*, Dallas, TX, ASME, **DSC-Vol. 61**, pp. 45-54.

Goldstein, H., 1980, Classical Mechanics, Addison-Wesley, Reading, MA.

Hogan, N., Krebs, H. I., Charnnarong, J., Srikrishna, P. and Sharon, A., 1992, "MIT-MANUS: A workstation for manual therapy and training," *Proc. Telemanipulator Technology*, Boston, ed. H. Das, SPIE, pp. 161-165.

Hollerbach, J. M., Cohen, E. C., Thompson, W. B., Freier, R., Johnson, D. E., Nahvi, A., Nelson, D. D. and II, T. V. T., 1997, "Haptic interfacing for virtual prototyping of mechanical CAD designs," *Proc. Design for Manufacturing Symposium*, Sacramento, CA, American Society of Mechanical Engineers.

Howe, R. D. and Cutkosky, M. R., 1993, "Dynamic tactile sensing: perception of fine surface features with stress rate sensing," *IEEE Transactions on Robotics and Automation*, Vol. 9, No. 2, pp. 140-151.

Keller, J. B., 1986, "Impact with Friction," *ASME Journal of Applied Mechanics*, Vol. 53, pp. 1-4.

Khalil, H. K., Teel, A. R., Georgiou, T. T., Praly, L. and Sontag, E., 1996, "Stability," in *The Control Handbook*, W. S. Levine, ed., CRC Press, Inc., pp. 889-908.

Klatzky, R., Lederman, S. and Reed, C., 1989, "Haptic Integration of Object Properties: Texture, Hardness, and Planar Contour," *J. of Exp. Psychology: Human Perception and Performance*, Vol. 15, No. 1, pp. 45-57.

LaBudde, R. A. and Greenspan, D., 1976, "Energy and momentum conserving methods of arbitrary order for the numerical integration of equations of motion, Part II," *Numerical Mathematics*, Vol. 26, pp. 1-16.

Lin, M. C. and Gottschalk, S., 1998, "Collision detection between geometric models: a survey," *Proc. Conference on Mathematics of Surfaces*, The Institute of Mathematics and its Applications, accepted for publication.

Lotstedt, P., 1984, "Numerical Simulation of Time-Dependent Contact and Friction Problems in Rigid Body Mechanics," *SIAM J. Sci. Stat. Computing*, Vol. 5, No. 2, pp. 370-393.

Millman, P. A., Stanley, M. and Colgate, J. E., 1993, "Design of a high performance haptic interface to virtual environments," *Proc. IEEE Virtual Reality Annual International Symposium*, Seattle, pp. 216-222.

Minsky, M. D. R., 1995, "Computational Haptics: The Sandpaper System for Synthesizing Texture for a Force-Feedback Display," , Ph.D. Thesis, Media Lab, MIT.

Mirtich, B. and Canny, J., 1994, "Impulse-based Dynamic Simulation," *Proc. Workshop on Algorithmic Foundations of Robotics*, Boston, MA, ed. K. Goldberg, P. Halperin, J. C. Latombe and R. Wilson, A.K. Peters.

Nahvi, A., Nelson, D. D., Hollerbach, J. M. and Johnson, D. E., 1998, "Haptic manipulation of virtual mechanisms from mechanical CAD designs," *Proc. International Conference of Robotics and Automation*, Leuven, Belgium, IEEE, pp. 373-380.

O'Modhrain, S. and Gillespie, B., 1997, "The Moose: A Haptic User Interface for Blind Persons," *Proc. The Third WWW Conference*, Santa Clara, CA.

Rosenberg, 1993, "Virtual Fixtures: Perceptual Tools for Telerobotic Manipulation," *Proc. IEEE Virtual Reality Annual International Symposium (VRAIS '93)*, Seattle, WA, IEEE, pp. 76-82.

Routh, E. J., 1905, Dynamics of a System of Rigid Bodies, Dover Publications, New York.

Salcudean, S. E. and Vlaar, T. D., 1994, "On the Emulation of Stiff Walls and Static Friction with a Magnetically Levitated Input/Output Device," *Proc. International Mechanical Engineering Exposition and Congress*, Chicago, IL, ed. C. J. Radcliffe, ASME, **DSC 55-1**, pp. 303-310.

Sasaki, Y. K., 1976, "Variational deisgn of finite-difference schemes for initial value problems with an integral invariant," *Journal of Computational Physics*, Vol. 21, pp. 270-278.

Simo, J. C. and Wong, K. K., 1991, "Unconditionally Stable Algorithms for Rigid Body Dynamics that Exactly Preserve Energy and Momentum," *International Journal for Numerical Methods in Engineering*, Vol. 31, pp. 19-52.

Slater, M. and Usoh, M., 1993, "Presence in Immersive Virtual Environments," *Proc. IEEE Virtual Reality Annual International Symposium*, Seattle, Washington, **1**, pp. 90-96.

Smith, C. E., 1991, "Predicting Rebounds Using Rigid-body Dynamics," *Transactions of the ASME*, Vol. 58, pp. 754-758.

Stewart, P., Chen, Y. and Buttolo, P., 1997, "Direct integration of haptic user interface in CAD systems," *Proc. Internation Mechanical Engineering Congress & Exhibition*, Dallas, TX, ASME, **DSC-Vol. 61**, pp. 93-99.

Stronge, W. J., 1990, "Rigid Body Collisions with Friction," *Proceedings of the Royal Society of London*, Vol. A431, pp. 169-181.

Wang, Y. and Mason, M. T., 1992, "Two-Dimensional Rigid-Body Collisions with Friction," *Journal of Applied Mechanics*, Vol. 59, pp. 635-642.

Zilles, C. and Salisbury, K., 1995, "A Constraint-Based God Object Method for Haptic Display," *Proc. International Conference on Intelligent Robots and Systems*, Pittsburgh, PA, IEEE/RSJ.

VITA

J. Michael Brown grew up in Palo Alto, CA. He received the B.S. degree in 1992 the M.S. degree in 1995, and the Ph.D. in 1998, all at Northwestern University in Mechanical Engineering. He will begin working in September 1998 at HT Medical, Inc., located in Rockville, MD. His research interests include haptic interface, computational dynamics, medical robotics, and teleoperation.

PUBLICATIONS

Brown, J. M. and Colgate, J. E., 1998, "Minimum Mass for Haptic Display Simulations," *Proc. International Mechanical Engineering Congress and Exhibition*, Anaheim, CA, ASME, accepted for publication.

Brown, J. M. and Colgate, J. E., 1997, "Passive Implementation of Multibody Simulations for Haptic Display," *Proc. International Mechanical Engineering Congress and Exhibition*, Dallas, TX, ASME, **DSC-61**, 85-92.

Colgate, J. E., Stanley, M. C. and Brown, J. M., 1995, "Issues in the Haptic Display of Tool Use," *Proc. IEEE/RSJ International Conference on Intelligent Robots and Systems*, Pittsburgh, **3**, 140-145.

Brown, J. M. and Colgate, J. E., 1994, "Physics-based Approach to Haptic Display," *Proc. Topical Workshop on Virtual Reality*, Houston, Texas, International Symposium on Measurement and Control in Robotics, **1**, 101-106.

Colgate, J. E. and Brown, J. M., 1994, "Factors Affecting the Z-width of a Haptic Display," *Proc. International Conference on Robotics and Automation*, San Diego, CA, IEEE, **4**, 3205-10.